이학박사학위논문

Half-metallic Ferromagnetism of perovskite oxide Sn-doped $SrRuO_3$

주석이 도핑된 $SrRuO_3$ 페로브스카이트 산화물의 반쪽금속 강자성체 연구

2015년 2월

서울대학교 대학원

계산과학 협동과정

김 남 욱

Half-metallic Ferromagnetism of perovskite oxide Sn-doped $SrRuO_3$

주석이 도핑된 $SrRuO_3$ 페로브스카이트 산화물의 반쪽금속 강자성체 연구

지도교수 유 재 준

이 논문을 이학박사 학위논문으로 제출함

2014년 10월

서울대학교 대학원

계산과학 협동과정

김 남 욱

김남욱의 이학박사 학위논문을 인준함

2014년 12월

위 원 장 신 동 우 (인)

부위원장 유 재 준 (인)

위 원 강 명 주 (인)

위 원 민 홍 기 (인)

위 원 한 명 준 (인)

Half-metallic Ferromagnetism of perovskite oxide Sn-doped $SrRuO_3$

Namwook Kim

Supervised by

Professor Jaejun Yu

A Dissertation

Submitted to the Faculty of

Seoul National University

In Partial Fulfillment of

the Requirements for the Degree of

Doctor of Philosophy

December 2014

Interdisciplinary Program of Computational Science and Technology

Graduate School

Seoul National University

Abstract

In this thesis, we investigate the electronic structure and properties of $SrRuO_3$ as a candidate of half-metallic ferromagnets. We will suggest two methods modulating the band structure of $SrRuO_3$ to become half-metallic ground states.

The first method is the doping of Sn atoms as substitute for Ru atoms. Due to the excellent band positioning between Ru $4d$ t_{2g} bands and Sn 5s bands, only small decrease of Ru $4d$ t_{2g} majority bandwidth can induce the half-metallic band structure of $SrRuO_3$. We carried out first-principles electronic structure calculations for the series of solid solutions $Sr(Ru_{1-x}Sn_x)O_3$ of orthorhombic perovskite adopting LSDA+U scheme with 1 eV of the effective value of on-site Coulomb interaction U_{eff} for Ru d-orbitals. We present the electronic structure and analysis of projected density-of-states of $Sr(Ru_{1-x}Sn_x)O_3$ for x = 1/8, 1/4, 1/2, 5/8, 3/4, 7/8. From the result, we can observe that the band width of Ru t_{2g} majority band decreased with Sn-doping. Since Sn $5s$ band has no overlap with Ru $4d$ band, the decreased hopping by B-site substituted Sn atoms narrows the bandwidth of Ru $4d$ t_{2g} band. And we also analyzed for the disorder in B-site atoms at fixed Sn-doping ratio. In the super-cell of $2\times2\times2$ times cubic perovskite unit cell, we calculated all the possible B-site

configurations of Ru atoms and Sn atoms. The Ru t_{2g} band in clustering types of defects are more dispersive than that in homogeneous types of defects. The averaged density-of-states over all possible B-site configurations at fixed Sn-doping ratio can suggest more reliable prediction for the phase transition to the half-metallic ground state. The calculated density-of-states shows half-metallic ferromagnetic ground states in the range of $0.6 < x < 0.75$ of Sn-doping. And the metal-insulator transition occurs at $x \sim 0.75$. The calculation including the spin-orbit coupling showed that the checker-boarded type of B-site defects has non-collinear spin structures but the total energy of the checker-boarded type is larger by 0.6 eV than the plane type.

The second method is an epitaxial strain on $SrRuO_3$. The change of lattice parameter can modulate the bandwidth of the material and we found that the expansion of volume by 9% can induce the half-metallic ground state of $SrRuO_3$. In experiments, the wide range of epitaxial strain can be given by the selection of substrate materials having different size of lattice. For better accuracy of calculated lattice parameters with experimental value, we used the PBEsol functional which can give improved bulk properties than PBE and LSDA. The band structure for 2.5% tensile epitaxial strain showed the maximally decreased Ru $4d$ t_{2g} bandwidth in LSDA+U and PBEsol+U calculations. Accidentally the best fitting substrate to the lattice size of 2.5% tensile strained $SrRuO_3$ was $SrSnO_3$ that is previously used by the doping material.

Our study is a new revenue in search of half-metallic materials in the perovskite family. Considering the potential application of half-metal in spintronics applications, we expect that the half-metallic Sn-doped $SrRuO_3$, when realized, can contribute to the development of devices and technology in spintronics.

Keywords: half-metallic ferromagnet, perovskite oxide, density functional theory calculations, on-site Coulomb interactions, $SrRuO_3$

Student Number: 2004-30166

Contents

List of Figures

Chapter 1

Introduction

The half-metallic ferromagnets (HMF) are unusual materials which show metallic property in one spin channel and insulating property in the other spin channel. After the pioneering work on the Mn-based Heusler alloys by de Groot and co-wokers[1], it was generally accepted as a new class of materials and investigated for its possible memory and spintronic device applications. Since theoretical investigations are not restricted by realistic problems, there have been many attempts in searching for new half metallic materials[2, 3]. However, since the experimental verification of half-metallicity is difficult, so far NiMnSb seems to be the only proven HMF, which has gathered enough evidences for its half-metallic ferromagnetism[3].

In addition to Heusler alloys, perovskite oxides has attracted a lot of attention as a promising class of materials for half metallic ferromagnets. Recent advances in making various hetero structures and controlling the stoichiometry and the ordering of elements has

made it possible to satisfy the need of complex electronic structures having both metallic and insulating characters in a system. One of the nearest realization of HMF was in doped manganites like $La_{0.66}$ $Ca_{0.33}MnO_3$ and $La_{0.7}Sr_{0.3}MnO_3$, where the double-exchange mechanism for the doped carrier leads to the HMF state and eventually to the colossal magnetoresistance behavior[2, 4]. Picking up the idea of double-exchange ferromagnetism in manganites, new forms of double perovskite structures have been suggested. The first series of double perovskites like Sr_2FeMoO_6, Sr_2FeReO_6, Sr_2CrWO_6, Sr_2CrFeO_3, and La_2VMnO_6 were predicted in which the B-site magnetic ion is substituted by another magnetic ion so that an ordered double perovskite structure can be stabilized[5~9]. Also suggested were a double doping of A- and B-sites in La(Sr,Ca,Ba)$VRuO_6$[10] as well as the doping of magnetic B-site ion with non-magnetic ions in Sr_2Fe(Sn,Ti,Zr)O_6[11]. An ordered double perovskite system has been considered as a promising candidate as a HMF materials as Sr_2FeMoO_6 was reported to be half-metallic exhibiting intrinsic tunneling-type magneto-resistance at room temperature. Unfortunately, however, the anti-ferromagnetic ordering between B-site ions, i.e., Fe^{3+} and Mo^{5+} ions is crucial to the realization of half-metallicity. Thus even a small amount of disorder may kill the half-metallicity in such double perovskite systems.

So far there is no simple cubic perovskite shown to be a half metallic system except $PdCrO_3$, which has recently been predicted

to be a first simple perovskite-type HFM[12]. Despite that prestine $SrRuO_3$ is a well-known ferromagnetic metal with Tc = 150 K[13], Katsnelson and co-workers[3] has pointed out that $SrRuO_3$ has all the ingredients for HMF as a low spin state of Ru occurs with almost full t_{2g} majority spin band and partially filled t_{2g} minority spin band. While there was a theoretical claim based on the LDA+U calculation predicting a half-metallic ground state with Jahn-Teller distortion[14], there has been no experimental report of either Jahn-Teller distortion or half-metallicity[13]. Rondinelli and co-workers made an extensive theoretical investigation on the ground state properties of $SrRuO_3$ and concluded that the on-site Coulomb interaction parameter U_{eff} needs to be set to be larger than 2 eV to achieve the half-metallic ground state in $SrRuO_3$, which is inconsistent with the absence of orbital ordering in experiment as well as the theoretical estimation of U_{eff} by the self-interaction-correction calculation[15].

Here we will introduce the Sn-doping as effective method to give the half-metallic ground state in $SrRuO_3$. Also we will show that the half-metallicity in Sn-doped $SrRuO_3$ is stable for the B-site mixing disorder.

There was some studies about the electronic structure of epitaxially strained orthorhombic $SrRuO_3$ in which peoples are interested in the different magnetic state between $CaRuO_3$ and $SrRuO_3$. They calculated epitaxially strained orthorhombic $SrRuO_3$ and showed that the epitaxial strain induce the change of angles of

rotation and tilting of RuO_6 octahedra which is important for the change of the spin state from magnetic to non−magnetic. But in our study for searching the half−metallic state, we focused on the change of in−plane and normal directional lattice size and the relative effect with rotation and tilting of RuO_6 octahedra. At first we reproduced previously studied results[29] and after that we will introduce the half−metallic ground state of $SrRuO_3$ induced by epitaxial strain with LSDA+U and PBEsol+U results.

Chapter 2

Half-metallic Ferromagnetism in Perovskite $SrRuO_3$

2.1 Possibility to Half-metallicity in $SrRuO_3$

$SrRuO_3$ is unique $4d$ ferromagnetic oxide. Since its good metallic conductivity and good thermal property and suitable size for popular substrates, it is widely used for electrodes in thin film community.

In $SrRuO_3$ Ruthenium is tetravalent in this compound as RuO2, which is nonmagnetic metal with $4d$ electrons in the slightly split t_{2g} subband, but in $SrRuO_3$ a magnetic low-spin state occurs with a filled t_{2g} majority-spin band and a partially filled t_{2g} minority-spin band. With enough sizes of exchange splitting and crystal-field splitting energy, $SrRuO_3$ can be an ideal candidate of half-metallic ferromagnet.

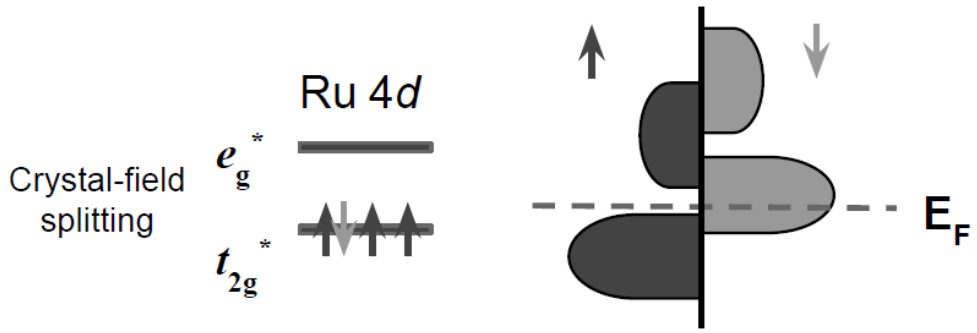

Figure 2.1: The spin-state of a tetra valent Ru ion. The fully occupied t_{2g} majority band and the partially occupied t_{2g} minority band have a possibility to become a half-metallic band structure.

2.2 Electronic structure of $SrRuO_3$

2.2.1 Crystal Structure of $SrRuO_3$

The crystal structure of $SrRuO_3$ has a series of structural transformations with temperature, from high symmetry cubic (Pm-3m, stable above 950 K) to tetragonal (I4/mcm, stable between 820 K and 950 K) to distorted orthorhombic structure (*Pbnm*) at low temperature.

The calculated lattice parameters of orthorhombic $SrRuO_3$ is slightly smaller than experimental values about 3.4% which is well-known underestimate of LDA.

2.2.1.1 Goldschmidt Tolerance Factor

$SrRuO_3$ has a perovskite structure, which is ABO_3 type stoichiometry. The perovskite structure consists of corner-sharing BO_6 octahedra and A-site ions residing in center-position of the cubic network of octahedra. The ideal perovskite is cubic (space group Pm-3m), but the relevant size between the cation and anion can make a distortion of structure or even a transition to another structure. The structural deformation of perovskite structure is simply formulated by the Goldschmidt tolerance factor. The first description of the tolerance factor for perovskite was made by Victor Moritz Goldschmidt in 1926. It was originally only used to describe perovskite structure, bur now tolerance factors are also used for ilmenite. Alternatively the tolerance factor can be used to calculate the compatibility of an ion with a crystal structure. The tolerance factor value of $SrRuO_3$ is 0.875, which is classified by $GdFeO_3$ type orthorhombic structure and has *Pbnm* space group.

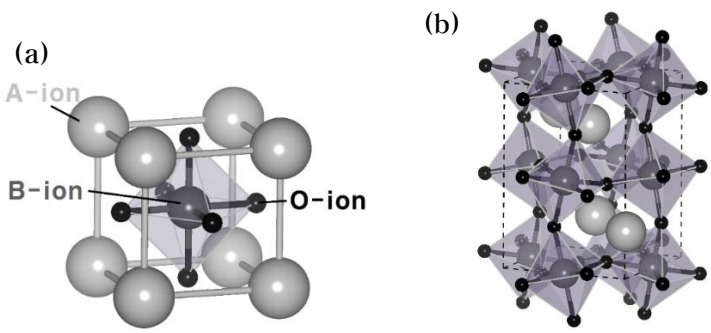

Figure 2.2: ABO_3 type of perovskite oxide structure. A-ion and B-ion are very different sizes of cations and O-ion is Oxygen. (a) Cubic perovskite unit-cell (b) Orthorhombic perovskite unit-cell

2.2.1.2 Irregular Lattice Distortion

From the table in Ref. 31, we can see that most of the *Pbnm* $GdFeO_3$-type structures have a < b < c, however $SrRuO_3$ is the only compound we know that have a > b. This has led to a confusion in the literature where one can find reports both of a > b and a < b; in the latter case, parameters are apparently switched to be consistent with overall trend in the $GdFeO_3$-type structures.

The in-plane lattice parameters of the *Pbnm* structure are not equal as a consequence of tilting. On the other hand the rotation does not change the ratio of a to b.

The reason for the anomaly in $SrRuO_3$ is that the oxygen octahedral are not regular square but rectangular. The a-axis lattice parameter of octahedral is about 2% longer than b-axis. These simple relations show that the internal distortions can be determined from fundamental parameters of the *Pbnm* structure. But the oxygen octahedral are not necessarily regular and the size of rectangular is free parameters unique for each material.

2.2.2 LSDA Calculation

To investigate the electronic structure and properties $SrRuO_3$ perovskite, we carried out density functional theory (DFT) calculations by using the full-potential projected augmented wave method[20] implemented in the VASP package[21, 22] within the

local spin density approximation (LSDA)[23]. The plane-wave energy cutoff 520 eV was used and the Brillouin-zone was sampled with a 10×10×8 k-point Monkhorst-Pack mesh[26]. We obtained optimized lattice structures as well as internal atomic positions through the relaxation steps below 5 meV/A of the Hellmann-Feynman forces. For the Brillouin-zone integrations, the tetrahedron method with Blöchl correction[27] was used for the better description of Fermi levels.

2.2.2.1 Cubic $SrRuO_3$

Cubic phase of $SrRuO_3$ is the metastable state above 950 K. The total energy of ferromagnetic ground state is lower than non-magnetic ground state. The density of states (DOS) is shown below. The valence band is composed of O 2*p* states hybridized with Ru 4*d* state. Oxygen states are found in lower region of valence band and Ru states are dominating at the Fermi energy. The large peak in the DOS near Fermi level is caused by the flat Ru t_{2g} bands near the Fermi level while the strongly hybridized e_g orbitals form broader bands ated the bottom of the valence and conduction bands. The Sr 4*d* states are found around 5 eV above the Fermi level.

The exchange splitting at Gamma point is 0.5 eV for Ru 4*d* states and 0.2 eV for O 2*p* states. The calculated magnetic moments per formula unit are found to be 1.09 μB.

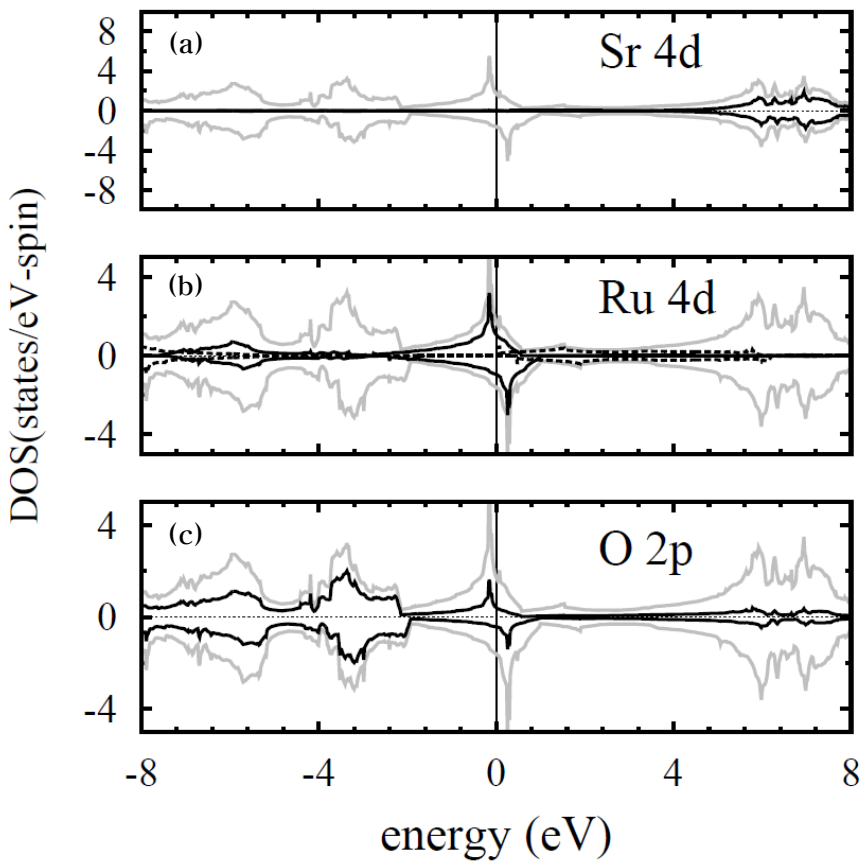

Figure 2.3: Projected density-of-states(pDOS) of cubic $SrRuO_3$ in LSDA calculation. The gray line is the total density. (a) The pDOS of the Sr atom. (b) The pDOS of the Ru atom. The bold line is the t_{2g} band and the dotted line is the e_g band. (c) The pDOS of the Oxygen atom.

2.2.2.2 Orthorhombic $SrRuO_3$

We calculated with the optimized LSDA lattice parameters for orthorhombic $SrRuO_3$. The ferromagnetic ground state is lower than the paramagnetic state and the calculated magnetic moment is about 0.8 μB. It is consistent with the experimental observation of ferromagnetic $SrRuO_3$ in the $GdFeO_3$ structure.

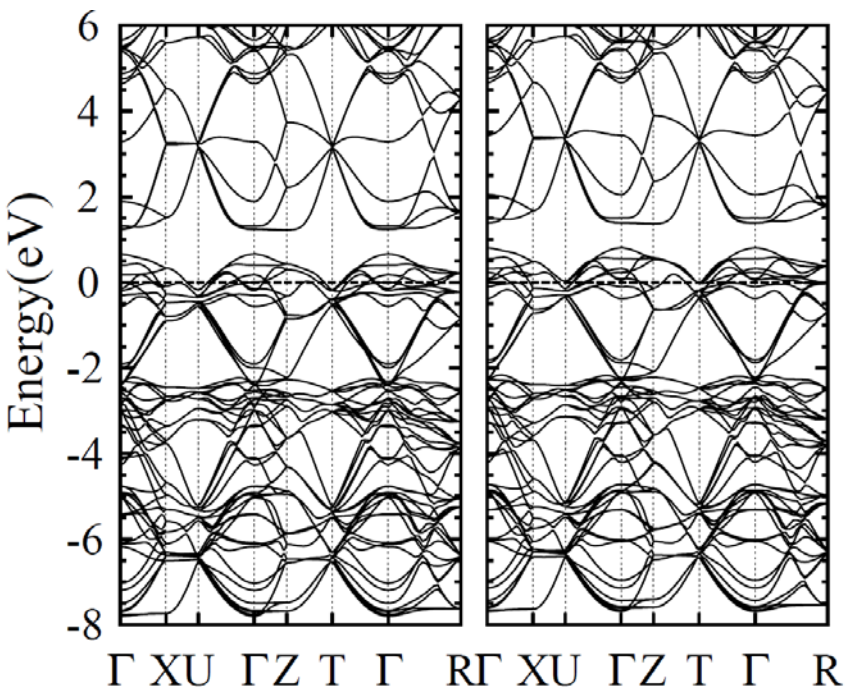

Figure 2.4: Band structures of majority and minority spins of orthorhombic $SrRuO_3$

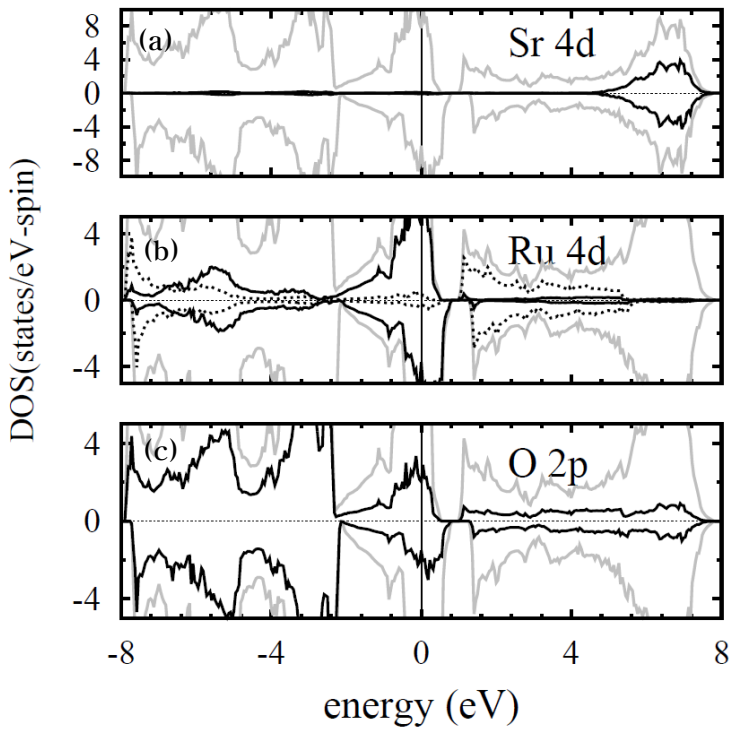

Figure 2.5: The pDOS of orthorhombic $SrRuO_3$ in LSDA calculation. The gray line is the total density. (a) The pDOS of the Sr atom. (b) The pDOS of the Ru atom. The bold line is the t_{2g} band and the dotted line is the e_g band. (c) The pDOS of the Oxygen atom.

In this band structure Fermi energy is set to 0 eV. Bands between −8eV and −6 eV are mainly formed by Ru e_g σ−bonding orbitals, and bands between −7 eV and −4 eV is by Ru t_{2g} π−bonding orbitals, and bands between −4 eV and −2 eV by oxygen $2p$ orbitals and bands between −2 eV and 1 eV are formed by Ru t_{2g} π−antibonding orbitals and bands between 1 eV and 5 eV by Ru e_g σ−antibonding orbitals. The magnitude of exchange splitting at Gamma point is about 0.2 eV and this is reduced comparing with the magnitude of cubic structure. But crystal field splitting is increased more than cubic

structure to give a pseudo-gap of 0.7 eV in both majority and minority band. That is from the effect of rotation and tilting of RuO_6 octahedrons by orthorhombic distortion.

The cubic $SrRuO_3$ has no rotation and tilting of RuO_6 octahedra, and the rotation and tilting of orthorhombic $SrRuO_3$ octahedra is about 8 degree and in $CaRuO_3$ the distortion is about twice larger increasing the overlap of Ru t_{2g} and e_g orbitals. Therefore hybridization between the t_{2g} and e_g bands makes the broadening of the logarithmic singularity of Ru t_{2g} bands in the density of states[28]. At the same time the bands become more narrowed and the gap between the antibonding t_{2g} bands and e_g bands grows.

2.2.3 LSDA+U Calculation

To investigate the electronic structure and properties $SrRuO_3$ perovskite, we carried out density functional theory (DFT) calculations by using the full-potential projected augmented wave method [20] implemented in the VASP package [21, 22] within the local spin-density approximation(LSDA) [23] and the LSDA+U scheme [24] as well. We adopted the spherically averaged form of the rotationally invariant LSDA+U introduced by Dudarev and co-workers, [25] where only one parameter $U_{eff} = U - J$ is used for the description of effective on-site Coulomb interactions for Ru d orbitals. In the LSDA+U calculations we employed U_{eff} = 1.0 eV for Ru d by benchmarking the calculated magnetic ground state against

the previous DFT works and experimental results [15]. The plane-wave energy cutoff of 520 eV was used and the Brillouin-zone was sampled with a 10×10×8 k-point Monkhorst-Pack mesh [26]. We obtained optimized lattice structures as well as internal atomic positions through the relaxation steps below 5 meV/A of the Hellmann-Feynman forces. For the Brillouin-zone integrations, the tetrahedron method with Blöchl corrections [27] was used for the better description of Fermi levels.

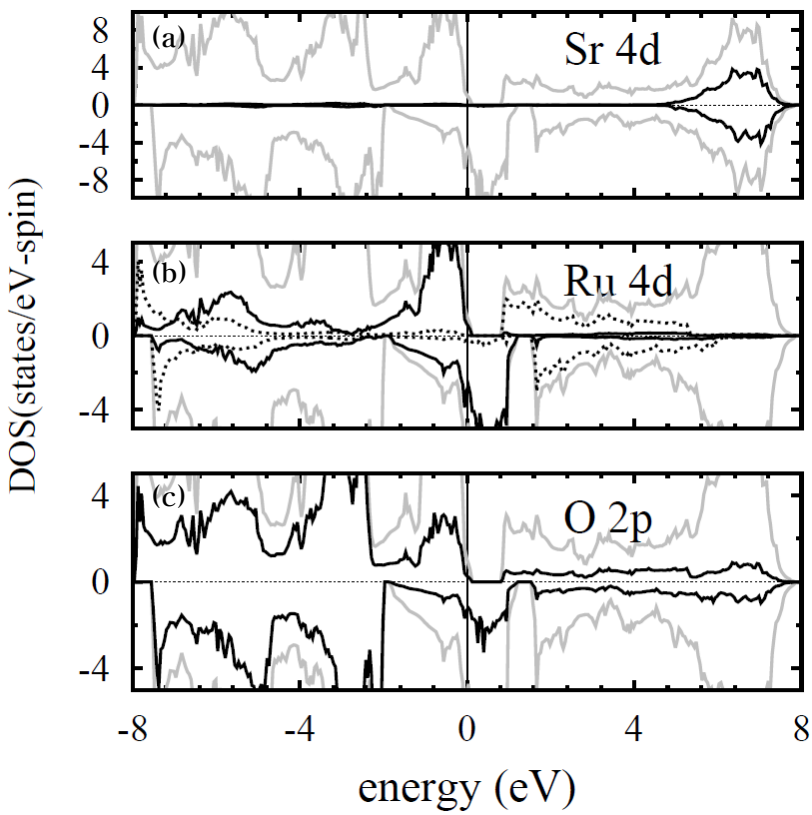

Figure 2.6; The projected density-of-states of orthorhombic $SrRuO_3$ in LSDA+U (U_{eff} = 1.0 eV) calculation. The gray line is the total density. (a) The pDOS of the Sr atom. (b) The pDOS of the Ru atom. The bold line is the t_{2g} band and the dotted line is the e_g band. (c) The pDOS of the Oxygen atom.

In this figure we shows the densities of states with U_{eff} = 1.0 eV for orthorhombic $SrRuO_3$. Compared with the LSDA result, the magnitude of exchange splitting is significantly increased by on-site coulomb energy correction to be close to the half-metallicity. The enhanced And the increased magnetic moment per formula unit is around 1.9 μB and enhanced exchange splitting of the Ru 4d states at Gamma is about 0.45 eV (~ 0.30 eV in LSDA). In addition the peak positions of the correlation included densities of states are in better agreement with the experimental spectra.

In Rondinelli's calculations, LSDA+U results and pseudo-SIC results are compared. And the pseudo-SIC shows better agreement with the PES in the bandwidth for the O 2p states between −8 eV and −4 eV. It is clear that both LSDA+U method and the pseudo-SIC suppress the t_{2g} states at the Fermi level and shift the center to higher energy (about −0.6 eV) and reproduce the incoherent feature better than LSDA.

2.2.3.1 U-dependent Half-metallicity

The magnitude of enhanced exchange splitting of Ru t_{2g} bands depends on the size of on-site coulomb energy which determines the energy difference between occupied and unoccupied sites in same orbitals. And the increased correlation narrows the bandwidth of Ru 4d t_{2g} majority band. That makes Ru t_{2g} majority band-edge to be shifted down to the Fermi energy. And the unoccupied Ru 4d e_g

bandwidth have less effect by increased correlation, so the pseudo-gap in majority band is maintained and increased, but in minority bands t_{2g} bandwidth is increased with larger correlation which leads to narrowed pseudo gap between t_{2g} and e_g bands. Above the 2.0 eV of U_{eff} value, $SrRuO_3$ have a ground state of half-metallic ferromagnet. But half-metallic states in $SrRuO_3$ is not observed experimentally

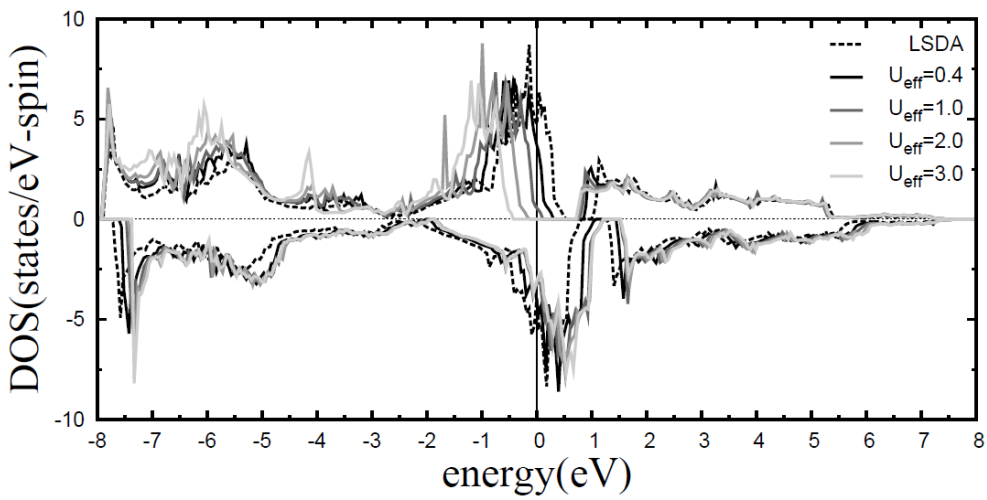

Figure 2.7: The DOS of SRO with different U_{eff} values. Ru t_{2g} majority bandwidth shifts with increasing U_{eff} value. For the U_{eff} larger than 1.0 eV, SRO has the half-metallic ground state. But that is not observed in experments.

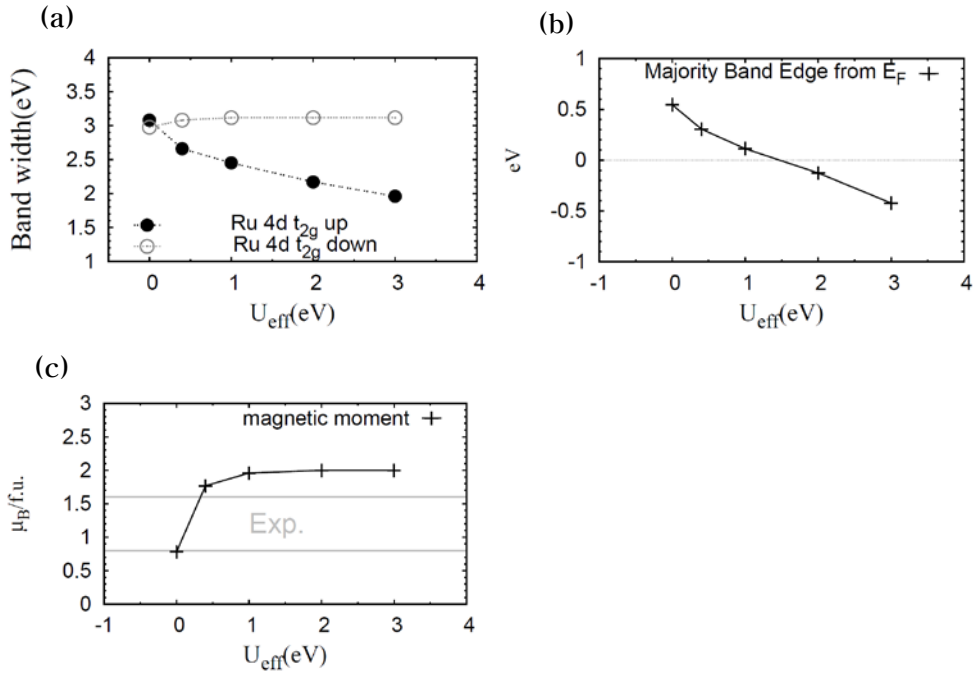

Figure 2.8: (a) Bandwidths of Ru t_{2g} majority and minority band with different U_{eff} value. Solid circles are up majority band and open circles are minority band. (b) The relative position of Ru t_{2g} majority band to the Fermi energy with different U_{eff} values. The Fermi energy set to 0 eV. (c) The change of the magnetic moment of a Ru atom. Through 1 eV of U_{eff} values SRO shows the integer magnetic moment.

The magnetic property is enhanced with increasing U_{eff} value. In this figure we shows the magnetic moment per formula unit as a function of increased correlation. For U_{eff} values larger than 0.4 eV, the magnetic moment is shown around $2\mu B$ which is the magnitude of the ideal low spin state of Ru ion. But in experiments the integer magnetic moment of $2\mu B$ was not observed and $1.66\mu B$ was obtained from extrapolation of high field limit results.

2.2.3.2 Determination of U_{eff} parameter

In general the parameter U_{eff} value is determined by fitting to the experimental values like an energy gap or magnetic moments. But in the case of $SrRuO_3$ both ways are not adaptable since $SrRuO_3$ is a metal not having an energy gap and the calculated magnetic moment is converged to $2\mu B$ above small U_{eff} value of 0.4 eV. Moreover experimentally observed magnetic moments are closer to the LSDA result.

In Rondinelli's paper, they determines the U_{eff} value as 1.0 eV by comparing the magnetic moment of cubic $SrRuO_3$ from LSDA+U and from the pseudo-SIC method which does not have parameters in calculation. In pseudo-SIC calculation, the magnetic moment of orthorhombic $SrRuO_3$ is $1.99\mu B$ which is comparable with LSDA+U results of every region above 0.4 eV of U_{eff} values. So they compare the magnetic moment of cubic $SrRuO_3$, but the cubic phase of $SrRuO_3$ exists above 950 K and its magnetic moment can not be observed by experiments. But we can not find another way better than that. In some papers, 2.5 eV of U_{eff} value was used for Ru $4d$ orbitals from the result of LCAO code, but in plane-wave code U_{eff} values larger than 2.0 eV shows half-metallic ground states in bulk orthorhombic $SrRuO_3$ which is not observed experimentally.

2.2.4 GGA and GGA+U Calculation

In calculations with the Perdew–Burke–Ernzerhof(PBE) version of the GGA exchange correlation functional, we can see the enhanced exchange splitting energy larger than LSDA result. The magnitude of enhanced exchange splitting energy is comparable with the result of LSDA+U calculation with 1.0 eV of U_{eff} value. With 1.0 eV of U_{eff} value, the Ru t_{2g} majority band is narrowed and band edge goes down to the Fermi level which shows larger correlation effect than LSDA+U results.

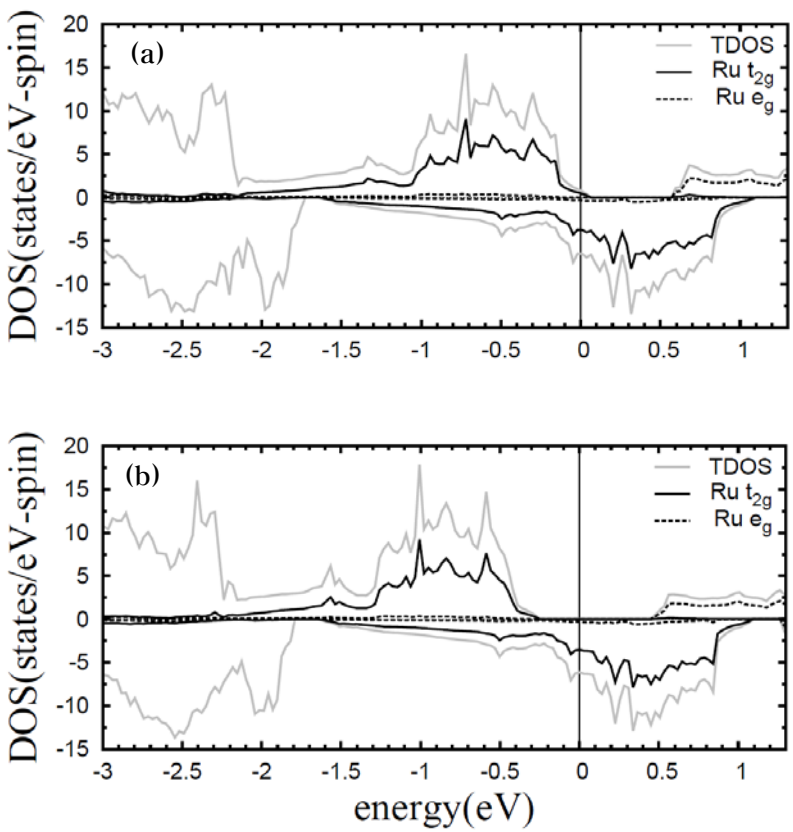

Figure 2.9: (a)GGA and (b)GGA+U(U_{eff} = 1.0 eV) calculations of SRO.

2.3 Sn-doped $SrRuO_3$

Perovskite $SrSnO_3$ is a semiconductor with 4.1 eV experimental energy gap, and it has various applications like transparent conducting oxides (TCOs) which are employed in the fabrication of the transparent electrodes for photovoltaic cells and organic light emitting diodes and used in lithium batteries and humidity sensors.

The aim of Sn-doping is to modulate the Ru t_{2g} majority bandwidth to become half-metallic band structure. The mixing of B-site atoms with Ru and Sn will compose localized Ru t_{2g} bands on the Fermi level which are surrounded by the gap of $SrSnO_3$. There is no overlap between Ru 4*d* bands and Sn 5*s*, that can reduces the hopping of Ru 4*d* electrons and narrows the bandwidth of occupied Ru 4*d* majority band.

2.3.1 Crystal Structure of $SrSnO_3$

The orthorhombic perovskite $SrSnO_3$ has *Pbnm* space group below 900 K which is the same with orthorhombic $SrRuO_3$.

To investigate the electronic structure and properties $SrRuO_3$ perovskite, we carried out density functional theory (DFT) calculations by using the full-potential projected augmented wave method [20] implemented in the VASP package [21, 22] within the local density approximation(LDA) [23]. The plane-wave energy cutoff of 520 eV was used and the Brillouin-zone was sampled with

a 10×10×8 k-point Monkhorst-Pack mesh [26]. We obtained optimized lattice structures as well as internal atomic positions through the relaxation steps below 5 meV/A of the Hellmann-Feynman forces. For the Brillouin-zone integrations, the tetrahedron method with Blöchl corrections [27] was used for the better description of Fermi levels.

The calculated lattice parameters are slightly larger than $SrRuO_3$ about 3.5% (LSDA) and the estimated lattice parameters are larger about 3.0%. The equivalent structure can give the structural stability after mixing of $SrRuO_3$ and $SrSnO_3$. LDA lattice parameters are smaller than experimental values that is from well-known trend of LDA's underestimate for lattice parameters.

Table 2.1: Lattice parameters of orthorhombic $SrSnO_3$ and orthorhombic $SrRuO_3$

Orthorhombic Lattice Parameters					
	$SrSnO_3$		$SrRuO_3$		
	LDA	Exp.	LSDA	Exp.	U_{eff} (1.0eV)
A	5.665	5.708	5.501	5.567	5.511
B	5.695	5.704	5.485	5.530	5.487
C	8.015	8.066	7.752	7.845	7.785
V	258.6	262.6	233.9	241.5	235.4

2.3.2 Electronic structure of $SrSnO_3$

$SrSnO_3$ has 4.1 eV of experimental band gap. But the calculated band gap is 1.9 eV which is smaller than the experimental value due to LDA's overestimation of the binding energy.

In this figure, Fermi energy is set to 0.0 eV. There are deep valence levels in the energy range about −20.0 eV formed by Sn d orbitals, between −18.0 eV and −13.0 eV mainly formed by Oxygen s and Sr p orbitals. The valence band between −9.0 eV and −5.0 eV is Sn s orbitals and the band between −5.0 eV and 0.0 eV are formed by Sn p orbitals and Oxygen p orbitals. The conduction band between 2.0 eV and 6.0 eV is formed by Sn s orbitals, and Sr d orbitals is above 6.0 eV.

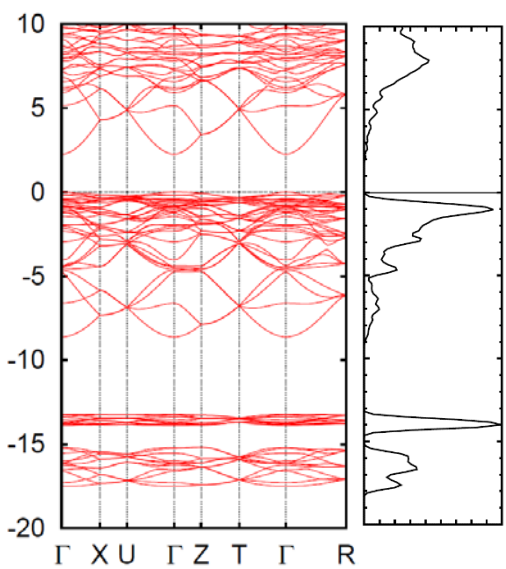

Figure 2.10: The band structure and DOS of $SrSnO_3$ In LDA. The calculated band−gap is 1.9 eV.

2.3.3 LSDA Calculation of $Sr(Ru_{1-x}Sn_x)O_3$

With VASP packages, we calculated the mixed structure of $Sr(Ru_{1-x}Sn_x)O_3$ for x=1/4, 1/2, 3/4 with orthorhombic unit cell which is a supercell of $\sqrt{2}\times\sqrt{2}\times 2$ times cubic perovskite unit cell in which the number of B-site atom is 4. The Brillouin zone was sampled with a $10\times10\times8$ k-points Monkhorst-Pack mesh and the unit-cell and internal geometries are fully optimized below the 5 meV/A of Hellmann-Feynman forces. Figures shows configurations of B-site mixing of Ru atoms and Sn atoms. Although one can find much more configurations for each doping ratio in a larger supercell, we first want to see the trend of change of electronic structures.

In the density of states of $Sr(Ru_xSn_{1-x})O_3$ show decreasing bandwidth of Ru 4*d* t_{2g} majority band. For x=0.5 and 0.75, the Ru 4*d* t_{2g} majority bands shift down below the Fermi level and the band structures show half-metallic ground states. In addition, both Ru t_{2g} minority band and e_g bands are also narrowed in bandwidth. That is differences with the result of decreased U_{eff} value in $SrRuO_3$ bulk structure in which only Ru t_{2g} majority band is narrowed. The exchange splitting energy is about 0.6 eV and is not changed by Sn-doping ratio. But spin polarization is increased by narrowing bandwidth of Ru t_{2g} bands. The Ru 4*d* t_{2g} majority band occupation increases with Sn-doping and the magnetic moment of one Ru atom is increased from 0.78 μB to 1.33 μB for x = 0.25 and 2.0 μB for x = 0.5 and 0.75. But another modulating factor of B-site configuration

can give some variations in the result. Although we did not show the results of another configuration of B-site atoms like line-type and plane-type for x = 0.5 case, for those cases Ru 4d t_{2g} majority bands are less narrowed and magnetic moments per Ru have rather smaller value of 1.14 μB and 1.51 μB than 2.0 μB of checker-boarder type.

For x=0.5 and 0.75, the e_g minority bands are highly localized around the Fermi level. That can lead to the need for beyond-DFT method since the neglected electron correlation energy in the LSDA framework is increased by Sn-doping.

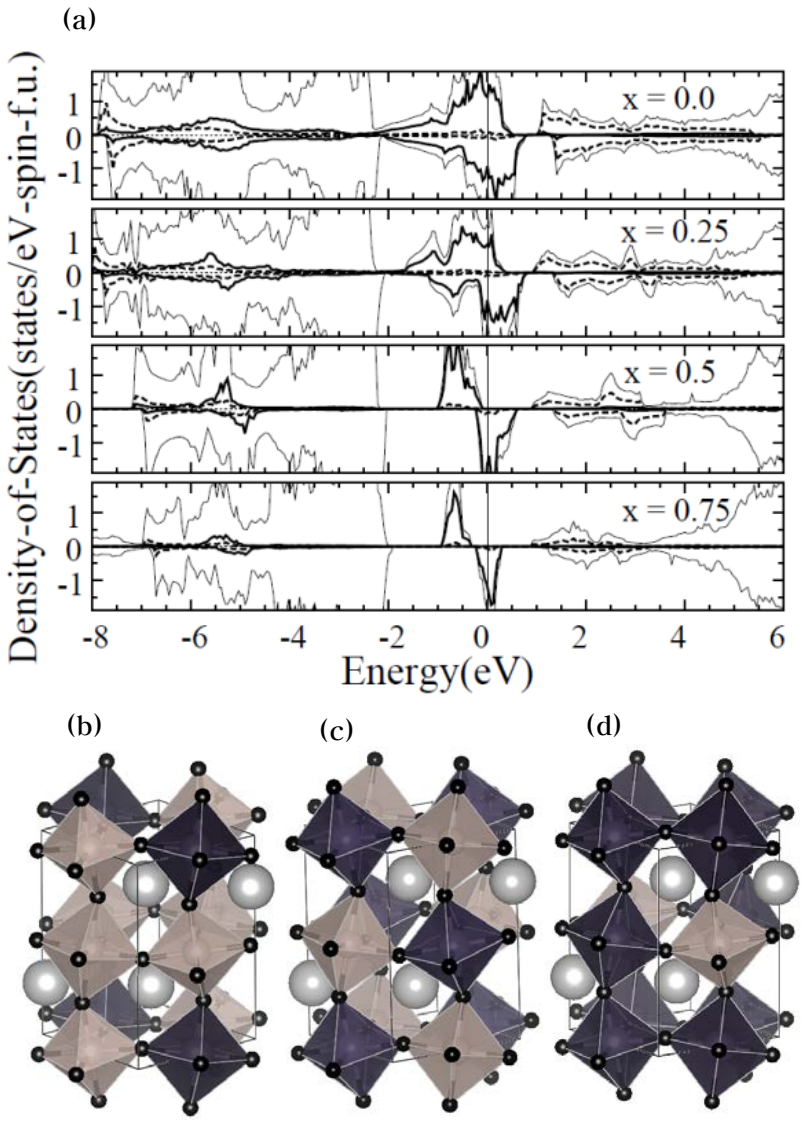

Figure 2.11: (a) DOSs of $Sr(Ru_{1-x}Sn_x)O_3$ for x = 0.0, 0.25, 0.5, 0.75 and B-site configuration for (b) x = 0.25 case and (c) x = 0.5 and (d) x = 0.75

2.3.4 LSDA+U Calculation of $Sr(Ru_{1-x}Sn_x)O_3$

With VASP packages, we adapted LSDA+U method of Dudarev's spherically averaged form to the calculation of $Sr(Ru_{1-x}Sn_x)O_3$ for x = 1/8, 1/4, 3/8, 1/2, 5/8, 3/4, 7/8. We used supercell of 2×2×2 times cubic perovskite unit-cell that have 8 B-site atoms. The Brillouin zone was sampled with 8×8×8 k-points Monkhhorst-Pack mesh and unit-cells and internal geometries are fully optimized below the 5 meV/A of Hellmann-Feynman forces. Used k-points are 6×6×6 by Monkhorst-pack. Used energy cutoff is 520 eV.

For each x value, the doping ratio of Sn atoms, all possible configurations of B-site in the used supercell were calculated. For x = 0.25, three types of configurations exist and for x = 0.5, five types of configurations exist and for x = 0.625, three types of configurations exists and for x = 0.75, also three types of configurations exist and for x = 0.875, just two types of configurations exist. In synthesizing process various structures are can be made in the material. We want to describe the status of real material by showing the density of states averaged over all possible configurations within fixed Sn-doping ratio. But we calculated possible configurations within 2×2×2 super-cell due to the limitation of our computational resource. Further calculations are needed within larger supercell.

In the averaged density of states, we can see the decrease of Ru t_{2g}

majority bandwidth according to the increasing Sn-doping. In spite of variation of B-site configurations, the decreasing tendency of Ru t_{2g} majority bandwidth is clearly observed. For x = 0.5, Ru t_{2g} majority band edge is just hanged on the Fermi energy. And for x = 0.625, Ru t_{2g} majority band is totally shifted down below the Fermi energy that shows the half-metallic ferromagnetic ground state. But for x = 0.75, the energy difference between occupied and unoccupied levels are increased by increased electron correlation energy. Therefore Ru t_{2g} minority band gap appears and the insulating ground state is obtained. In the $SrRuO_3$, Oxygen $2p$ orbitals have small amount of magnetic moments, since the electrons of Ru is itinerant. But electrons of Ru is more localized by Sn-doping, and Oxygen $2p$ orbitals are neutralized and the energy shift between majority and minority bands is disappeared with Sn-doping.

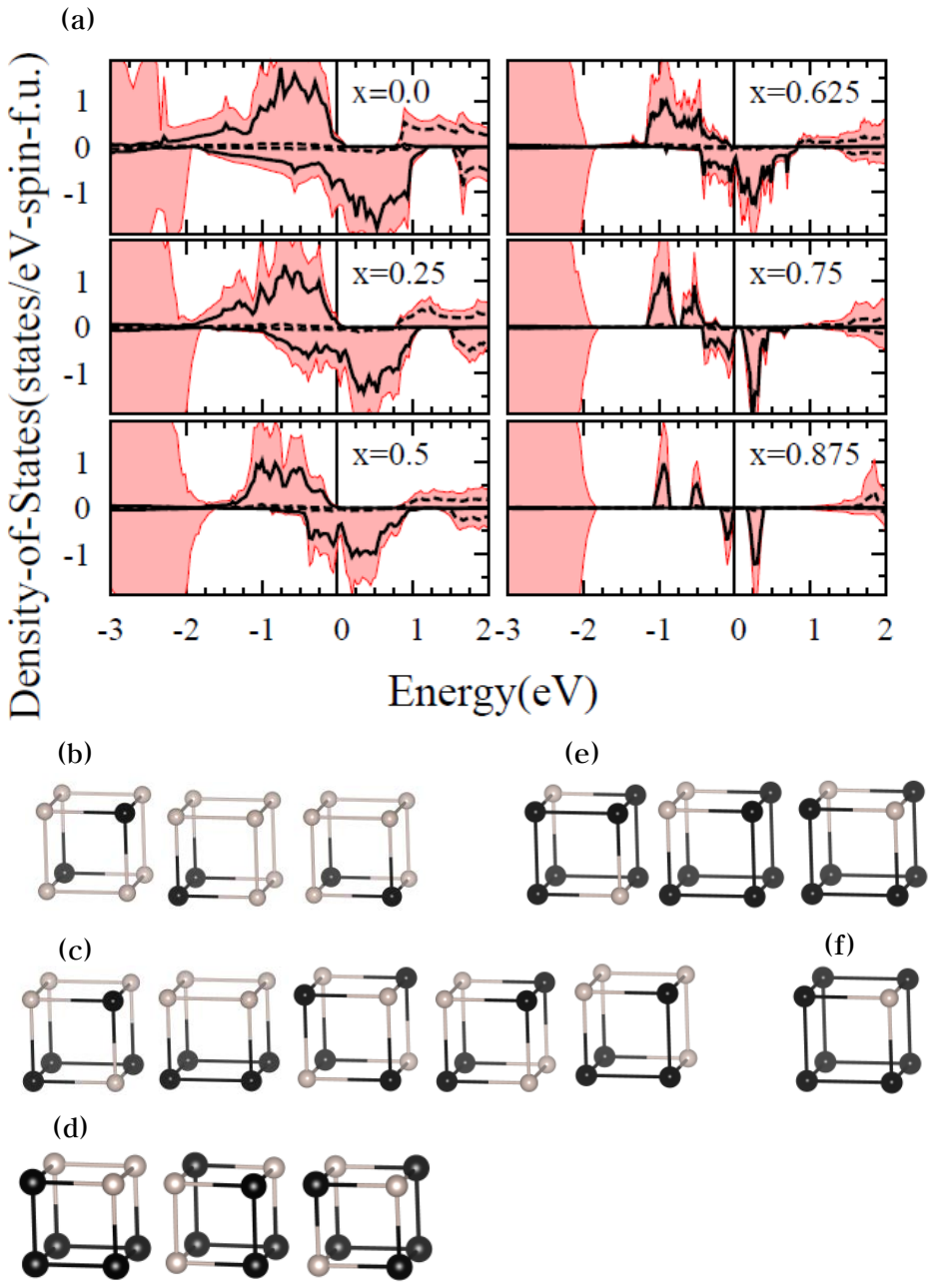

Figure 2.12: (a) Averaged DOSs for every configuration at fixed Sn−doping ratio in 2×2×2 super−cell. The pink area is the TDOS and the solid line is Ru t_{2g} band and the dotted line is Ru e_g band. All possible configurations (b) for x = 0.25 (c) for x = 0.5 and (d) for x = 0.625 and (e) for x = 0.75 and (f) for x = 0.875

2.3.5 Half-metallic and Metal-Insulator Transitions in $Sr(Ru_{1-x}Sn_x)O_3$

In the schematic picture of Ru 4*d* t_{2g} bands, we can see the transition from the ferromagnetic band structure to the half-metallic band structure and next to the insulating band structure. The transition between ferromagnetic metal and half-metal is modulated by majority bandwidth and also can be described by the position shift of majority band edge. And the transition between half-metal and insulator is controlled by the energy gap formation of minority band splitting.

Ru t_{2g} majority bandwidths for all configurations are ploted versus Sn-doping ratio with guiding line for mean values. The line of mean values of bandwidth shows linear dependence with Sn-doping ratio. But there is a dispersive variations with configuration dependency. The variation is most dispersive at x = 0.5 having the maximun difference between homogeneous structures and clustered structures. And the indexing order is arranged by lower total energy within fixed Sn-doping ratio. In all Sn-doping ratio, minimun total energy is given by the most clustered structure which has the maximun bandwidth.

The relative position to Fermi energy of Ru majority band edge ploted is directly showing the transition from metal to half-metal.

For x = 0.25, bandedge positions of all three configurations are

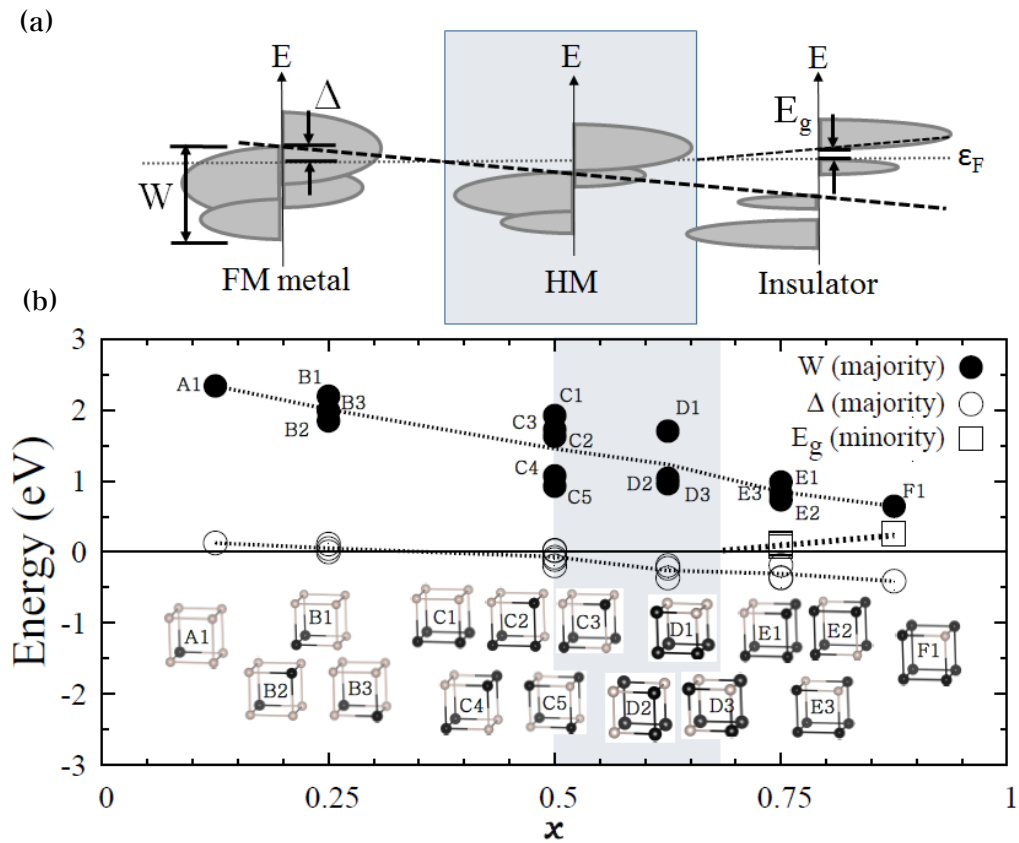

Figure 2.13: (a) The schematic description of phase transitions by the Ru t_{2g} majority bandwidth modulation. W is bandwidth of the Ru t_{2g} majority band and delta is the relative position Ru t_{2g} majority band-edge versus Fermi level and E_g is the band-gap of Sn-doped SrRuO3. (b) The guiding line is pointed on average values. The indexing orber is according to the lower total energy. And shaded region shows the half-metallic ground state of $Sr(Ru_{1-x}Sn_x)O_3$.

hanged on the Fermi level. For x = 0.5, bandedges of four configurations are totally shifted below the Fermi level, but only the case of plane type defects is still hanged on the Fermi level. Since its total energy is lowest of all, the half-metallic transition can not begin until 0.5 Sn-doping ratio. For x = 625, all three bandedges are set below the Fermi level, therefore the half-metallic ground state can be found in stable condition for defects disorder. And the critical point of metal to half-metal transition must be appear between 0.5 and 0.625 of Sn-doping ratio. For x = 0.75, all three configurations have energy gaps and they are larger than 0.1 eV. Therefore the transition of half-metal to insulator can appear between 0.625 and 0.75 of Sn-doping ratio.

2.3.6 B-site Configuration Dependency

With fixed Sn-doping ratio, we can have various configurations of B-sites of Sn atoms and Ru atoms. At x = 0.5 we have three types of configurations, plane type and line type and checker-boarded type. The difference of these types is the number of nearest neighbor of Ru atoms which controls the hoping of Ru 4*d* electrons. The plane type has four nearest neighbor Ru sites and the line type has 2 nearest neighbor Ru sites and the checker-boarded type has no nearest neighbor Ru site. Therefore the plane type configuration has maximum bandwidth of Ru t_{2g} bands and the checker-boarded type configuration has minimum bandwidth of Ru t_{2g} bands. That means more homogeneous mixing like the checker-boarded type is prior

than other configuration for making a half-metallic band structure.

In line type configuration, the formation of pseudo gap in t_{2g} minority band is larger than that in plane type configuration. That is from the orbital ordering of t_{2g} minority band is most strong in the plane type configuration since the Ru t_{2g} minority band has only one occupied electron so the d_{xy} orbital is much lower than the d_{xz} orbital and the d_{yz} orbital.

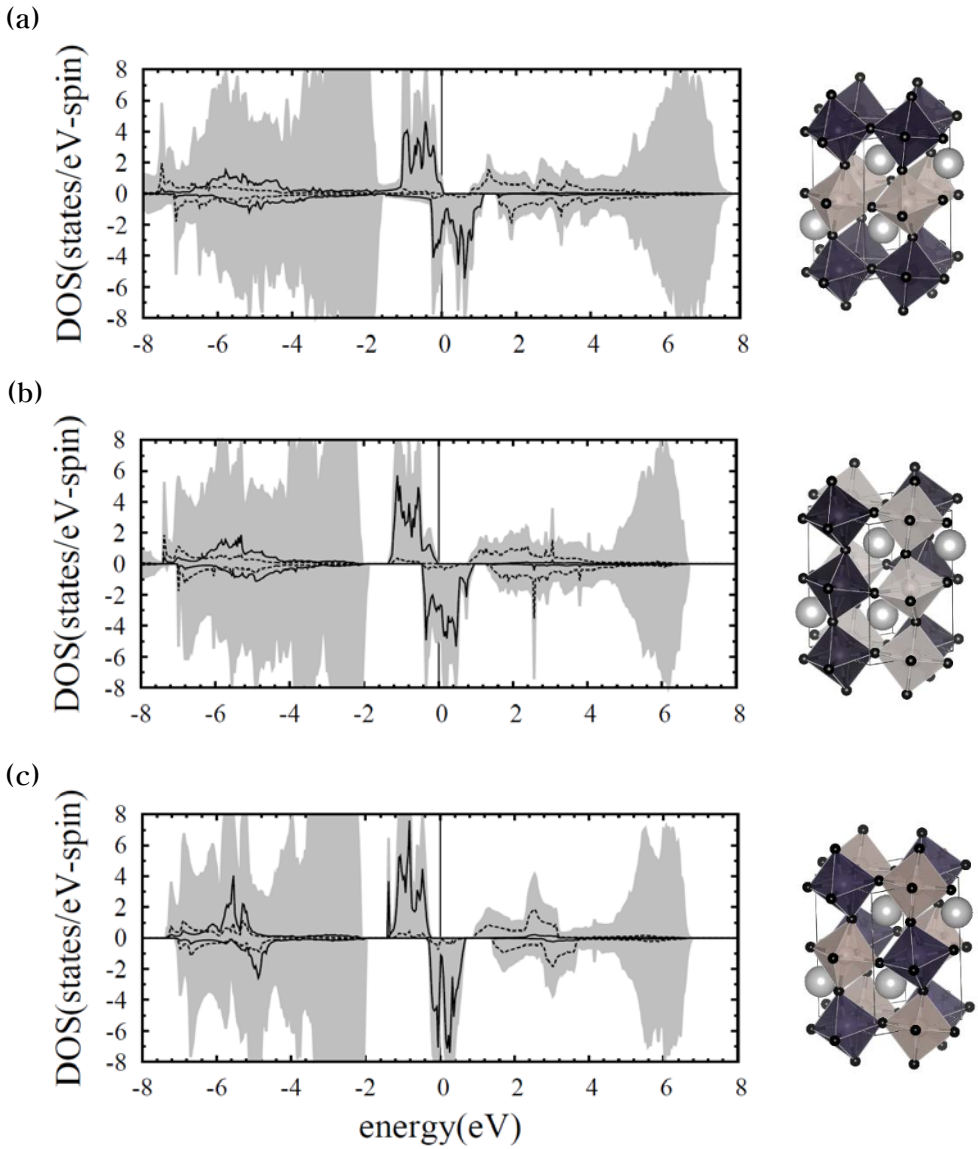

Figure 2.14: DOSs of $Sr(Ru_{1-x}Sn_x)O_3$ at x = 0.5. Shaded regions are TDOSs and solid lines are Ru 4d t_{2g} bands and the dotted lines are e_g bands. (a) plane type configuration (b) line type configuration (c) checker-boarded type configuration

2.3.6.1 Total Energy and Spin State

In the previous section, we showed that more homogeneous configuration is good for the formation of half-metallic band structure. And we calculated the total energy difference of those configurations and also calculated for spin states. And results show that the plane type configuration has lowest total energy and the ferromagnetic spin state is favored. The checker-boarded type configuration shows highest total energy and little difference between the ferromagnetic and the anti-ferromagnetic spin state. The anti-ferromagnetic ground state can destroy the half-metallic band structure and spin polarized transport. But the lowest total energy represents the least probability to appear in synthesized material.

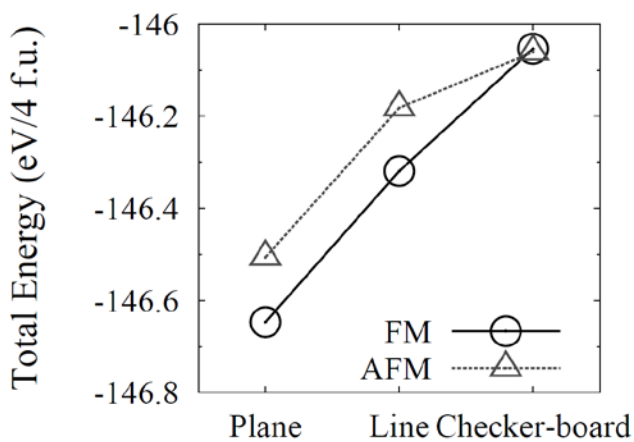

Figure 2.15: Total energies for spin-states and configurations at 0.5 of Sn-doping ratio.

2.3.6.2 Spin-orbit Coupling

Including the spin-orbit coupling, we calculated the total energy and the spin structure of each configuration. The selected configurations are calculated in $2\times2\times2$ supercell and $\sqrt{2}\times\sqrt{2}\times2$ supercell.

For all configurations except the checker-boarded type, spin structures are close to the collinear spin structure and average magnetic moment per Ru is larger than 1.9 μB. But the checker-boarded type configuration shows non-collinear spin structure and two spin vectors are vertically directed and the average magnetic moment for Ru is 1.5 μB. But total energy of the checker-boarded type configuration is still lowest of all configuration in the same Sn-doping ratio.

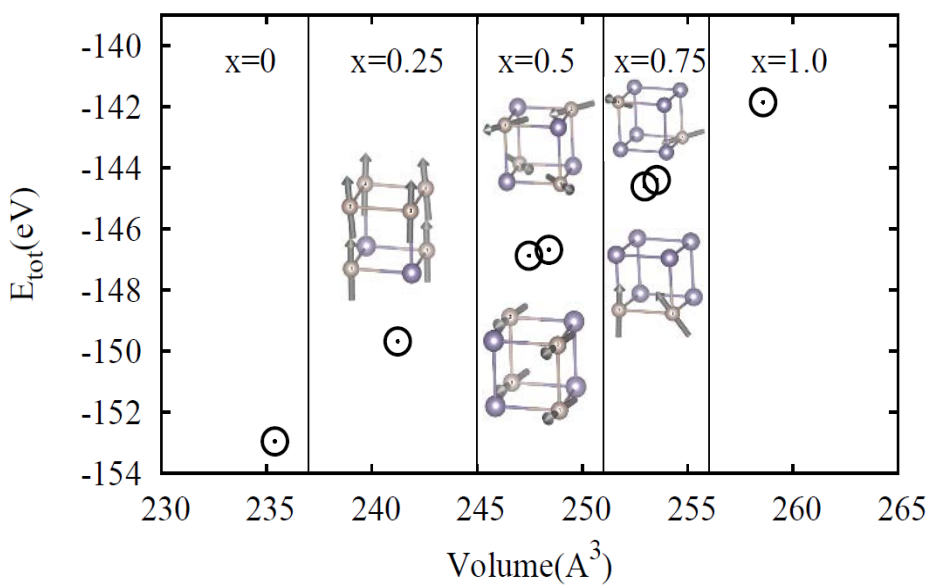

Figure 2.16: Spin structures from Spin-orbit coupling calculations

2.3.7 Lattice Expansion with Sn−doping

We calculated 3% volume expansion and 3% contraction of the orthorhombic $SrRuO_3$ and checked the change of the Ru t_{2g} bandwidth. Since the lattice size of $SrSnO_3$ is 3% larger than that of $SrRuO_3$ in calculation and the lattice size of $SrRuO_3$ is increased by Sn−doping. With contraction or expansion of lattice, internal geometry was optimized but the angles of ration and tilting of RuO_6 octahedron changed smaller than 1.0 degree. So we can see purely the lattice size effect. For t_{2g} majority bands, the bandwidth is decreased with 3% volume expansion and the band edge position goes down by 0.24 eV and sites below the Fermi level and shows the half−metallic band structure. The band center of t_{2g} majority band is not moved and the shift of band edge is totally from the reduction of bandwidth. For e_g majority bands, the difference of bonding and anti−bonding energy is decreased by 0.46 eV from the increased bond length and that makes the band edge of e_g majority band closer to the Fermi level.

And we also calculated the volume expansion and contraction for x = 0.5 Sn−doping case. Since lattice volumes of these configuration were already increased by Sn−doping, the expansion is set to the lattice volume of $SrSnO_3$ and the contraction is set to the lattice volume of $SrRuO_3$. For the plane type configuration, Ru t_{2g} majority bandwidth is decreased by 0.13 eV with volume expansion and become the half−metallic band structure. For the checker−boarded type configuration, Ru t_{2g} majority bandwidth is decreased by 0.05

eV which is much smaller than that of plane type configuration.

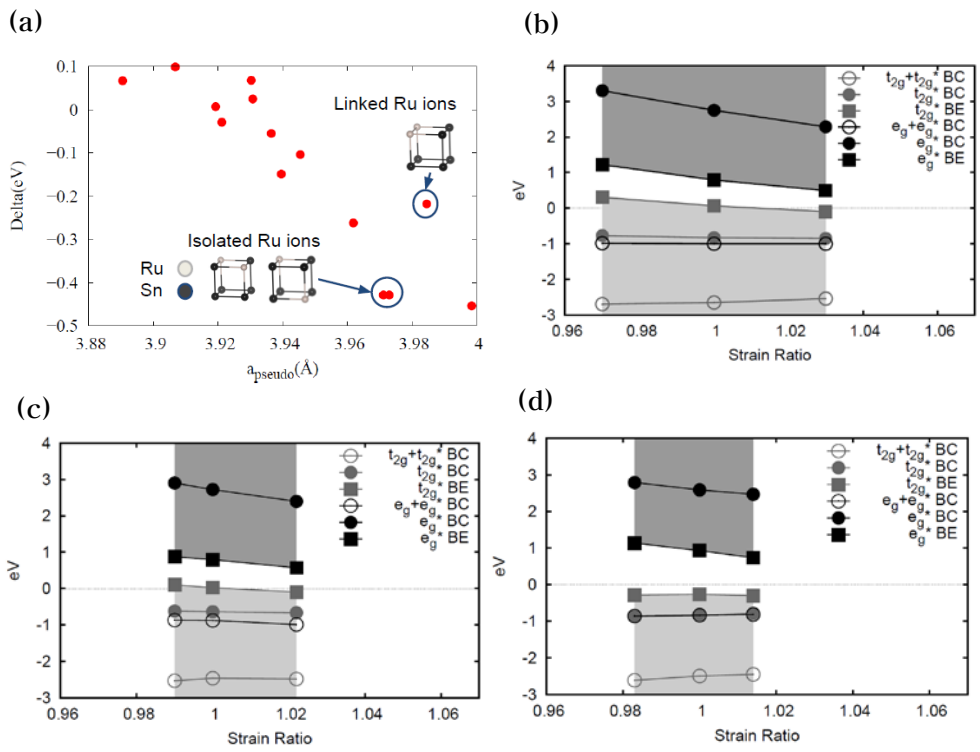

Figure 2.17: (a) Relative positions of band-edge to the Fermi level were arranged by the size of pseudo a-lattice vector. (b) Relative positions of band-edges and band-centers of t_{2g} and e_g bands with volume contraction and expansion in orthorhombic $SrRuO_3$ and (c) in the plane type of $SrRu_{0.5}Sn_{0.5}O_3$ and (d) in the checker-boarded type of $SrRu_{0.5}Sn_{0.5}O_3$

2.4 Epitaxial Strain on $SrRuO_3$

The orthorhombic $SrRuO_3$ has a possibility to be a half-metallic ferromagnet and Sn-doping can solve the problem of Ru t_{2g} bandwidth modulation. But we can see the lattice expansion also can play the same thing in the last section of previous chapter. In experiments the expansion of volume is hard to be controlled. By selections of substrate materials, in-plane strain can be adapted to epitaxially grown $SrRuO_3$ and in this chapter we will show the result of the bandwidth modulation by epitaxially strained $SrRuO_3$.

2.4.1 Structural Distortion by Epitaxial Strain

The epitaxial strain is a strain by fixed in-plane lattice size. Therefore the normal directional lattice will be changed. There was some studies about the electronic structure of epitaxially strained orthorhombic $SrRuO_3$ in which peoples are interested in the different magnetic state between $CaRuO_3$ and $SrRuO_3$. They calculated epitaxially strained orthorhombic $SrRuO_3$ and showed that the epitaxial strain induce the change of angles of rotation and tilting of RuO_6 octahedra which is important for the change of the spin state from magnetic to non-magnetic. But in our study for searching the half-metallic state, we focused on the change of in-plane and normal directional lattice size and the relative effect with rotation and tilting of RuO_6 octahedra.

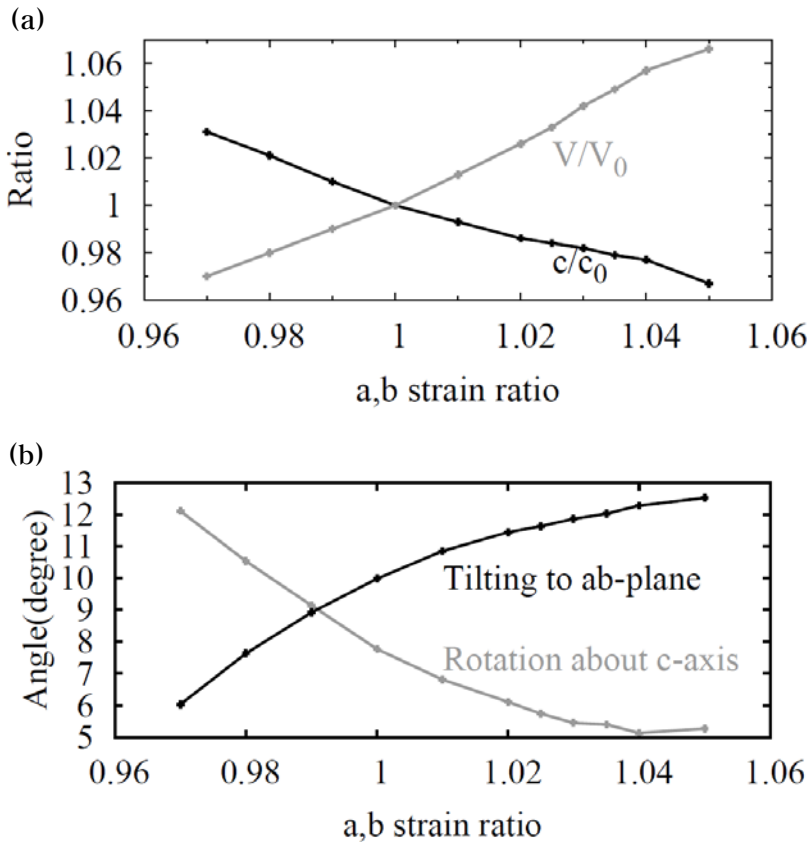

Figure 2.18: (a) The c−axis lattice and the volume of the unit−cell and (b) rotaion and tilting angles of the RuO_6 octahedron in epitaxial strain on $SrRuO_3$

The volume of the lattice is increased with increasing in−plane lattice tensile strain. The increased volume also can help the decrease of the bandwidth. But the size of normal directional lattice is linearly decreased with increasing in−plane lattice tensile strain, the decreased normal directional lattice is different with the case of the volume expansion and the opposite size change of normal directional lattice can cause the bandwidth increase than that of the volume

expansion case. But the opposite change of the other lattice to the strained lattice is consistent with the Poisson effect.

The rotation and tilting angles of the RuO_6 octahedron are also oppositely changed with in-plane lattice strain. The rotation angle of the RuO_6 octahedron is decreased with in-plane tensile lattice strain and the tilting angle is increased with in-plane tensile lattice strain. For non-magnetic spin state, rotation and tilting angles show different change with ferromagnetic spin state. But the total energy of non-magnetic ground state is larger than that of ferromagnetic ground state until the in-plane tensile strain is larger than 3.5%.

2.4.2 LSDA and LSDA+U Calculation

To investigate the electronic structure and properties epitaxially strained orthorhombic $SrRuO_3$, we carried out density functional theory (DFT) calculations by using the full-potential projected augmented wave method [20] implemented in the VASP package [21, 22] within the local spin-density approximation(LSDA) [23] and the LSDA+U scheme [24] as well. We adopted the spherically averaged form of the rotationally invariant LSDA+U introduced by Dudarev and co-workers, [25] where only one parameter $U_{eff} = U - J$ is used for the description of effective on-site Coulomb interactions for Ru d orbitals. In the LSDA+U calculations we employed U_{eff} = 1.0 eV for Ru d by benchmarking the calculated magnetic ground state against the previous DFT works and

experimental results [15]. The plane-wave energy cutoff of 520 eV was used and the Brillouin-zone was sampled with a 10×10×8 k-point Monkhorst-Pack mesh [26]. We obtained optimized normal directional lattice and internal atomic positions through the relaxation steps below 5 meV/A of the Hellmann-Feynman forces. For the Brillouin-zone integrations, the tetrahedron method with Blöchl corrections [27] was used for the better description of Fermi levels.

We calculated the total density of states for epitaxially compressive and tensile strain on the orthorhombic $SrRuO_3$ in the range from 3% of compressive to 3% tensile strain. For the epitaxially compressive strained $SrRuO_3$, both of bandwidths of Ru 4*d* t_{2g} bands and e_g bands are increased. The increased bandwidth is understood by the reduced volume which can increase the hopping of electrons of Ru. Also the increased repulsion energy raised the splitting of Ru 4*d* t_{2g} orbitals between bonding and anti-bonding energies. And next for the epitaxially tensile strained $SrRuO_3$, bandwidths of Ru 4*d* t_{2g} bands are slightly decreased by the increase of volume, but the bandwidth e_g bands are not decreased but increased. The decreased c-lattice can be more severe than the volume increasement. And the energy difference of t_{2g} orbitals between bonding and anti-bonding is increased by the enlarged lattice volume. For further anlysis we calculated the projected density-of-states of epitaxially strained orthorhombic $SrRuO_3$.

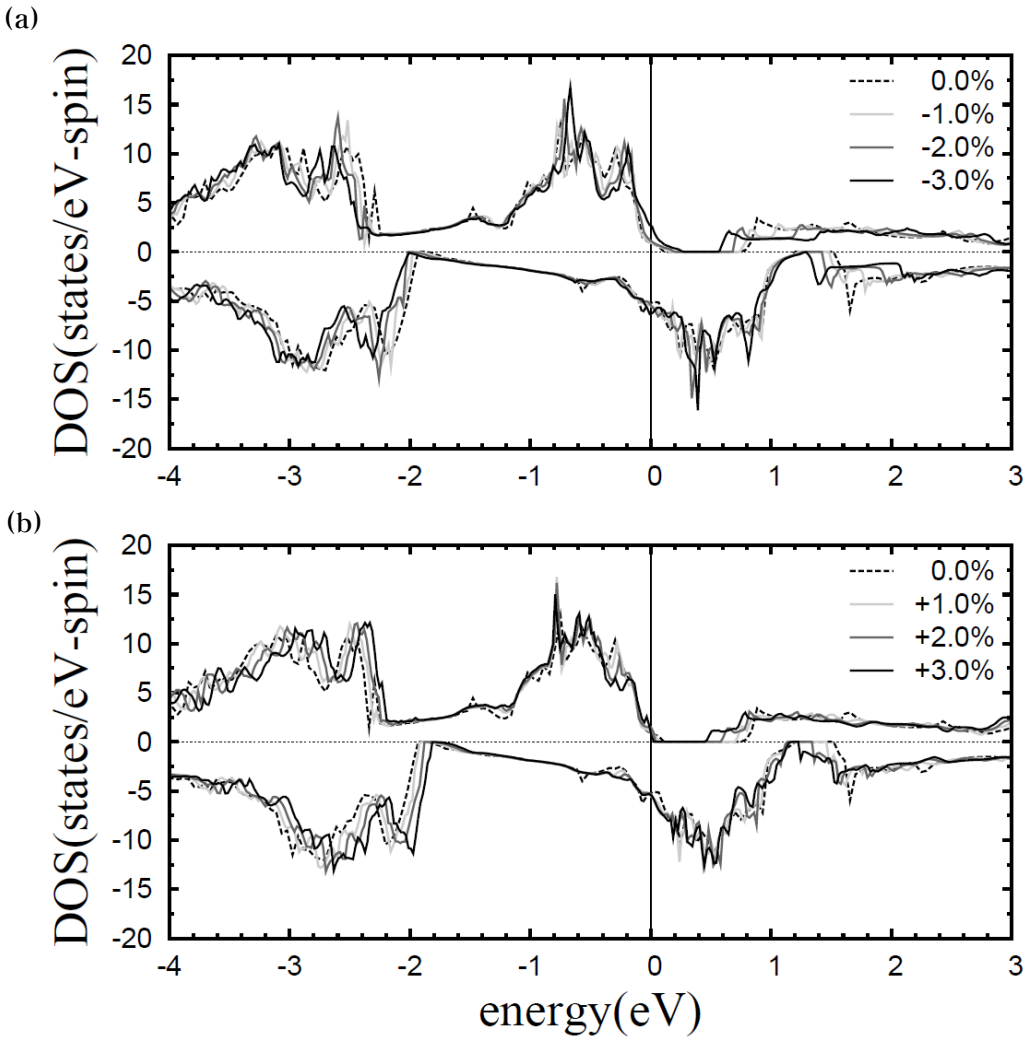

Figure 2.19: Total density−of−states of (a) the compressive and (b) the tensile epitaxial strain on the $SrRuO_3$.

The orbital ordering of Ru 4*d* t_{2g} and e_g orbitals is shown in the projected density of states of Ru 4*d* in orthorhombic $SrRuO_3$.

In the 3% compressive in-plane strain case, the normal directional lattice size is increased but the bandwidth of d_{z2} is not decreased but increased. That is the effect of the tilting of RuO_6 octahedron. The tilting angle was changed from 10 degree in no strain case to 5 degree in compressive in-plane strain case. The decreased tilting angle to recover the bond length with Oxygen gives decreased hybridization between Ru t_{2g} orbitals and e_g orbitals which narrows the bandwidth of d_{z2} orbitals. And the decreased rotation angle of RuO_6 octahedron to recover the bond length with Oxygen also gives increased hybridization between Ru t_{2g} orbitals and e_g orbitals which enlarges the bandwidth of d_{x2-y2} orbitals.

In the 3% tensile in-plane strain case, the same as compressive in-plane strain case not d_{z2} orbitals but d_{x2-y2} orbitals are increased in bandwidth. But t_{2g} orbitals are showing different feature with compressive in-plane strain case. The bandwidth of t_{2g} majority band is decreased than that of no strain case. It is relative to the increased volume. The contribution to hybridization between the decreasing rotation angle and the increasing tilting angle seems to have a minimum value near the 3% tensile in-plane strain region. The decrease of rotation angle of RuO_6 octahedron by 7 degree makes about 0.2 eV down shift of t_{2g} band edge by comparing the 3% compressive strain case and the 3% tensile strain case.

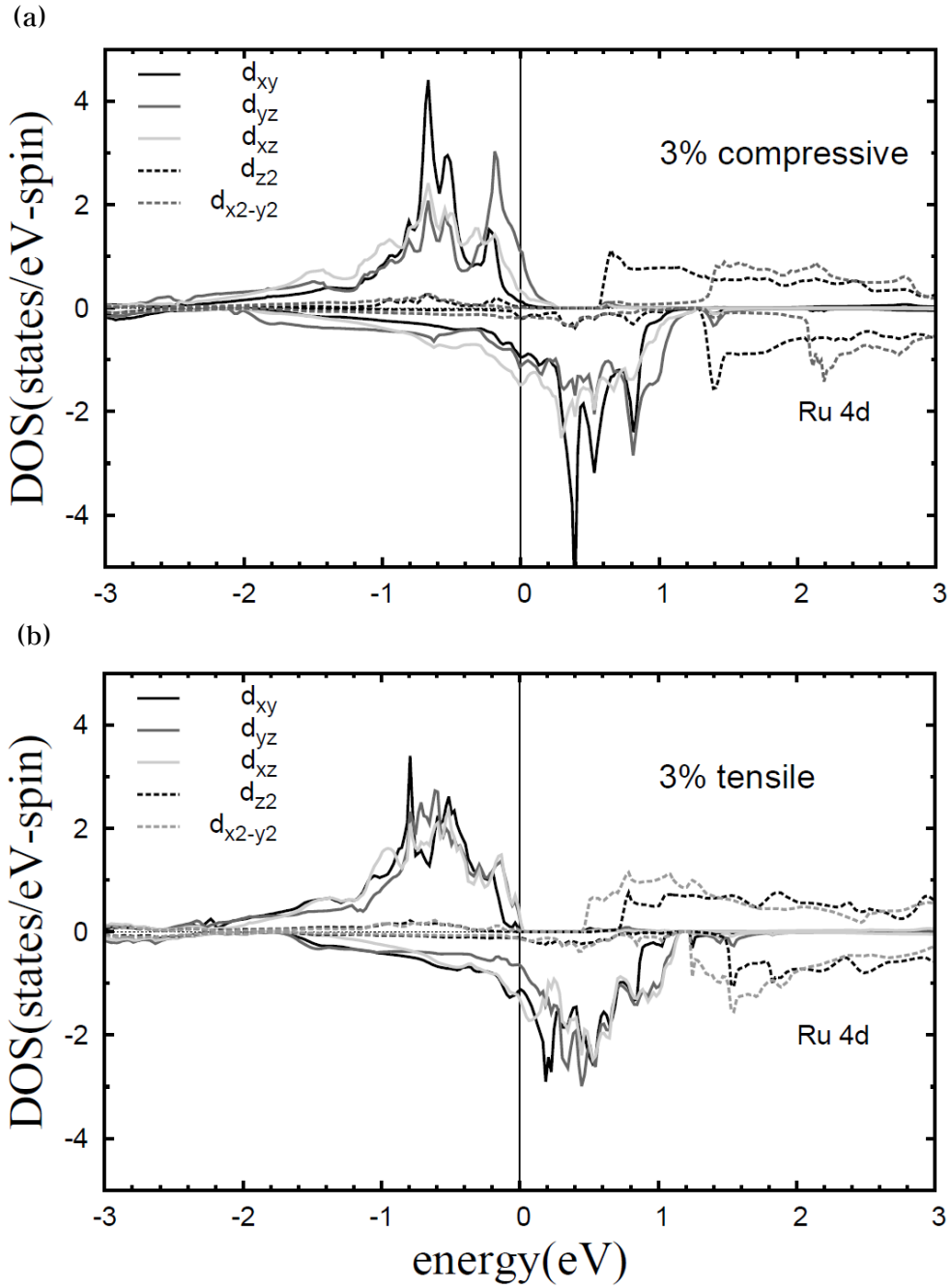

Figure 2.20: Projected DOSs of (a) 3% compressive epitaxial strained $SrRuO_3$ and (b) 3% tensile epitaxial strained $SrRuO_3$.

Further calculations show that the optimized strain ratio for minimal hybridization is 2.5% tensile in-plane strain, in which the maximally down shifted Ru t_{2g} majority band edge appears and the half-metallic band structure was found. You can see the t_{2g} majority band edge is down below the Fermi level at 2.5% tensile in-plane strain.

For the next step, we searched substrate materials whose in-plane lattice is fitted to that of the 2.5% tensile in-plane strained $SrRuO_3$ for the prediction of a suitable substrate material modulating the orthorhombic $SrRuO_3$ to the half-metallic material. Frequently used substrates have less size of lattice than the orthorhombic $SrRuO_3$ in the data from LSDA calculations. Accidentally $SrSnO_3$ used by doping material in my previous study has most close lattice size with that of 2.5% tensile in-plane strained $SrRuO_3$.

Still there are two problems, first the position of Ru t_{2g} majority band edge in the epitaxially strained $SrRuO_3$ is very sensitive to the value of U_{eff} and, second the region of strain ratio showing the half-metallic is so narrow that the error of LSDA calculation can exceed the range of prediction. For the first problem, the increased volume of tensile strained $SrRuO_3$ can increase the localization of Ru $4d$ electrons in which the U_{eff} value of Ru $4d$ orbitals may have a larger value and the decreased t_{2g} majority bandwidth supports the argument. For the second problem, we calculated with PBEsol exchange correlation functional which can give better prediction for lattice parameters of bulk materials.

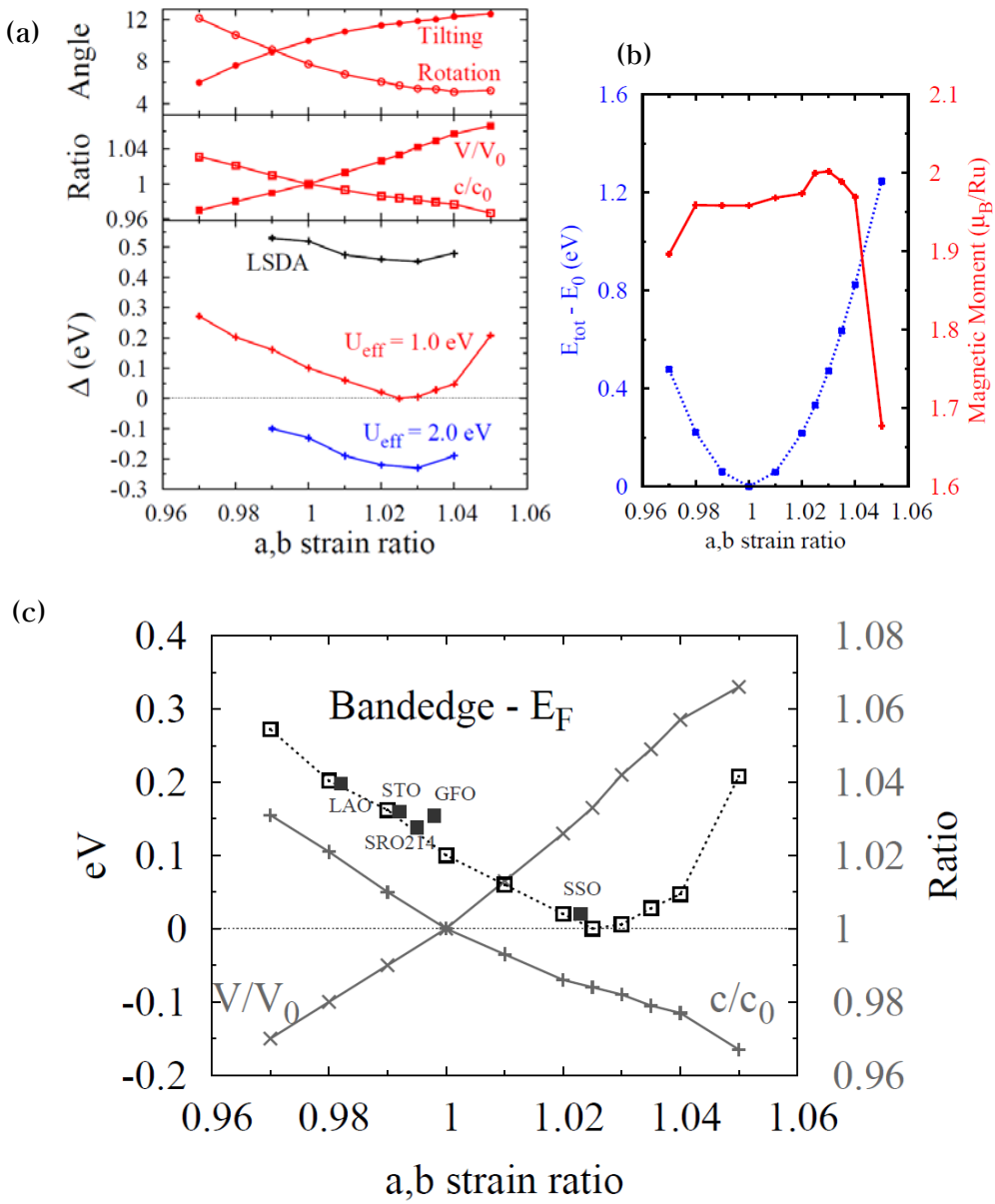

Figure 2.21: (a) Relative positions of Ru t_{2g} majority band−edge to the Fermi level with epitaxial strains and U_{eff} values of 0 eV, 1.0 eV and 2.0 eV. (b) The magnetic moment and the total energy with epitaxial strains. (c) Relative band−edge positions to the Fermi level in 1.0 eV of U_{eff} value with eptaxially strained $SrRuO_3$, and LDA lattice data of substrates are shown to comparison with that of strained $SrRuO_3$.

2.4.3 PBEsol and PBEsol+U Calculation

The PBEsol functional is the improved version of PBE functional to give better prediction for bulk properties like lattice parameters. Since parameters of original PBE functional are fitted to the description for the molecular system that is opposite to the uniform electron gas limit.

By comparing the calculated lattice volume of orthorhombic $SrRuO_3$ among LSDA and PBE and PBEsol, the LSDA lattice volume of $SrRuO_3$ is 4% smaller than that of the experimental value and the PBE lattice volume is 4% larger than that and PBEsol lattice volume is only 0.5% larger than the experimental value.

We also checked the U_{eff} value for PBEsol functional and calculated the Ru t_{2g} majority band edge shift by U_{eff} values. The electron correlation energy for PBEsol functional was larger than that of LSDA. At $U_{eff} > 0.2$ eV, the band edge went down below the Fermi level that is shown in LSDA at $U_{eff} > 2.0$ eV. The U_{eff} value of PBEsol fitted to LSDA+U results was 0.1 eV with comparing the position of the Ru t_{2g} majority band edge.

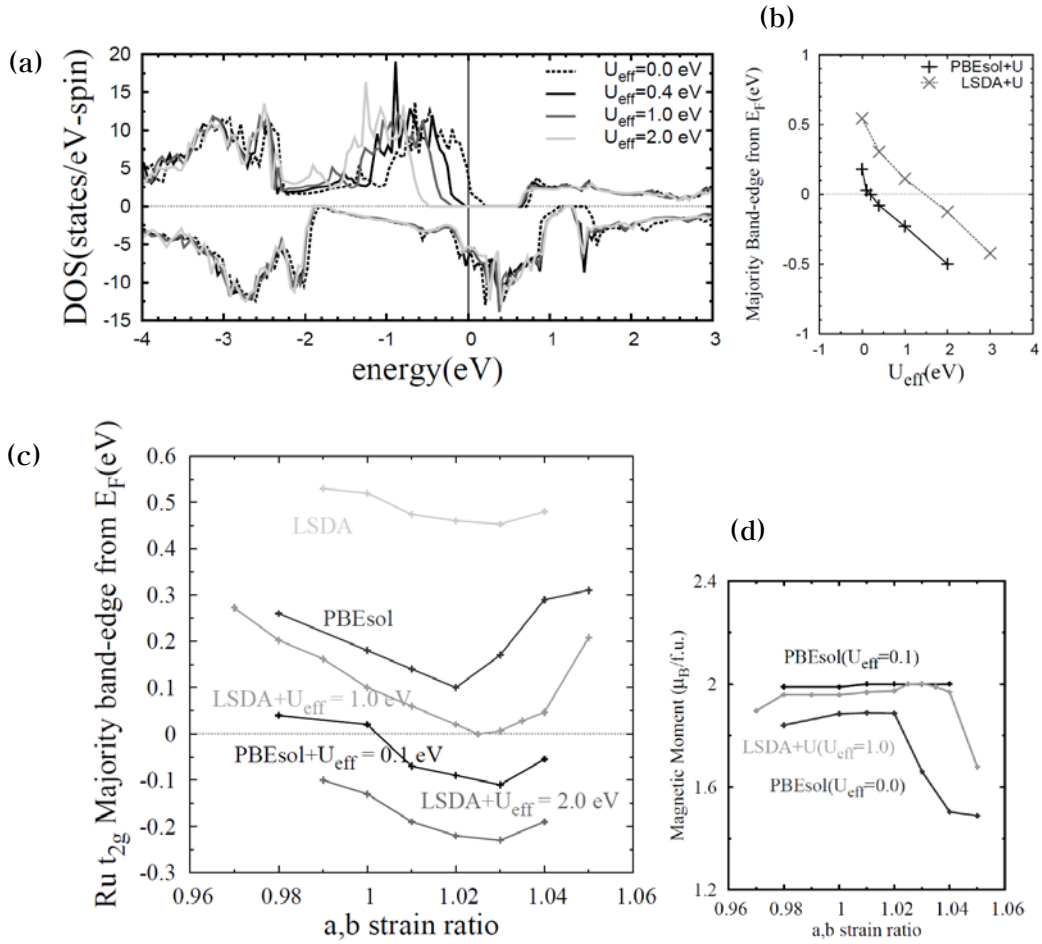

Figure 2.22: (a) TDOSs of $SrRuO_3$ in PBEsol+U (b) Relative band-edge positions by U_{eff} values (c) Relative band-edge positions with LSDA+U and PBEsol +U (d) magnetic moments in LSDA+U and PBEsol+U

The plot of Ru t_{2g} majority band edge position relative to Fermi level shows the range of strain ratio in which the epitaxially strained bulk $SrRuO_3$ has the half-metallic ground state. The PBEsol calculation with U_{eff} = 0 eV did not show the half-metallic state in all the range of strain ratio. And the PBEsol+U calculation with 0.1 eV of U_{eff} value showed the half-metallic state at 0.1 ~ 0.3% tensile in-plane strain

cases. Although the curve of the Ru t_{2g} majority band edge positions is so sensitively shifting by U_{eff} values, the minimum position of curves are in the range from 2% to 4% tensile epitaxial strain..

Chapter 3

Summary and Perspectives

In unique $4d$ ferromagnetic oxide $SrRuO_3$, Ruthenium ion has a magnetic low-spin state with a filled t_{2g} majority-spin band and a partially filled t_{2g} minority-spin band. But the size of exchange splitting is not enough to be the half-metallic ferromagnet.

The Sn-doping modulates the Ru t_{2g} majority bandwidth to become half-metallic band structure. The mixing of B-site atoms with Ru and Sn will compose localized Ru t_{2g} bands on the Fermi level which are surrounded by the gap of $SrSnO_3$. There is no overlap between Ru $4d$ bands and Sn $5s$, that can reduces the hopping of Ru $4d$ electrons and narrows the bandwidth of occupied Ru $4d$ majority band.

In the LSDA+U result, we can see the transition from the ferromagnetic band structure to the half-metallic band structure and next to the insulating band structure. The transition between ferromagnetic metal and half-metal is modulated by majority bandwidth and also can be described by the position shift of majority band edge. And the transition between half-metal and insulator is

controlled by the energy gap formation of minority band splitting. . The critical point of metal to half-metal transition appear between 0.5 and 0.625 of Sn-doping ratio and the transition of half-metal to insulator can appear between 0.625 and 0.75 of Sn-doping ratio.

But there is a dispersive variation of Ru t_{2g} bandwidth with the B-site configuration. The variation is most dispersive at x = 0.5 having the maximun difference between homogeneous structures and clustered structures. In all Sn-doping ratio, minimun total energy is given by the most clustered structure which has the maximun bandwidth.

Including the spin-orbit coupling, all configurations except the checker-boarded type have the collinear spin structures and average magnetic moments per Ru with larger than 1.9 μB. But the checker-boarded type configuration shows non-collinear spin structure and two spin vectors are vertically directed and the average magnetic moment for Ru is 1.5 μB. But total energy of the checker-boarded type configuration is lowest of all configuration in the same Sn-doping ratio.

The orthorhombic $SrRuO_3$ has a possibility to be a half-metallic ferromagnet and Sn-doping can solve the problem of Ru t_{2g} bandwidth modulation. Also we can see the lattice expansion can play the same thing. In experiments the expansion of volume is hard to be controlled. By selections of substrate materials, in-plane strain can

be adapted to epitaxially grown $SrRuO_3$.

We showed that 2.5% tensile epitaxial strain can induce the half-metallic ground states in orthorhombic $SrRuO_3$ in which the rotation and tilting of RuO_6 octahedron is important for bandwidth modulation. Accidentally the best size matching substrate material was the $SrSnO_3$ which was used for doping. The PBEsol+U calculation also give the consistent results with LSDA+U.

Still we could not find an experiment to search the half-metallic state in the $SrRuO_3$. But in our collaboration group there was similar experiment to searching for a p-type transparent conducting oxide. In that data we hopes to find some meaningful relation with the half-metallic ferromagnet.

Our study is a new revenue in search of half-metallic materials in the perovskite family. Considering the potential application of half-metal in spintronics applications, we expect that the half-metallic Sn-doped SrRuO3, when realized, can contribute to the development of devices and technology in spintronics.

Bibliography

[1] R.A. de Groot, F. M. Mueller, P. G. van Engen, and K. H. J. Buschow, Phys. Rev. Lett. 50, 202 (1983).

[2] W. E. Pickett and J. S. Moodera, Phys. Today 54, 39 (2001).

[3] M. I. Katsnelson, V. Y. Irkhin, L. Chioncel, A. I. Lichtenstein, and R. A. de Groot, Rev. Mod. Phys. 80, 315 (2008).

[4] J.-H. Park, E. Vescovo, H.-J. Kim, C. Kwon, R. Ramesh, and T. Venkatesan, Nature 392, 794 (1998).

[5] K.-I Kobayashi, T. Kimura, H. Sawada, K. Terakura, and Y. Tokura, Nature 395, 677 (1998).

[6] K.-I Kobayashi, T. Kimura, Y. Tomioka, H. Sawada, and K. Terakura, Phys. Rev. B 59, 11159 (1999).

[7] H.-T. Jeng and G. Y. Guo. Phys. Rev. B 67, 094438 (2003).

[8] K.-W. Lee and K.-H. Ahn. Phys. Rev. B 85, 224404 (2012).

[9] W. E. Pickett, Phys. Rev. B 57, 10613 (1998).

[10] J. H. Park, S. K. Kwon, and B. I. Min, Phys. Rev. B 65, 174401 (2002).

[11] I. R. Shein, V. L. Kozhevnikov, and A. L. Ivanovskii, JTEP Letters 82, 220 (2005).

[12] H.-S. Jin and K.-W. Lee, Phys. Rev. B 84, 172405 (2011).

[13] J. Janbayasi, J. Phys. Soc. Jpn. 41, 1876 (1976).

[14] H.-T. Jeng, S.-H Lin, and C.-S. Hsue, Phys. Rev. Lett. 97, 067002 (2006).

[15] J. M. Rondinelli, N. M. Caffrey, S. Sanvito, and N. A. Spaldin, Phys. Rev. B 78, 15510 (2008).

[16] K. W. Kim, J. S. Lee, T. W. Noh, S. R. Lee, K. Char, Phys. Rev. B 73, 125109 (2005).

[17] J. Kim, J. Y. Kim, B. G. Park, and S. J. Oh, Phys. Rev. B 77, 085118 (2008).

[18] P.-A. Lin, H.-T. Jeng, and C.-S. Hsue, Phys. Rev. B 77, 085118 (2008).

[19] H.-M. Christen, L. Boatner, L. English, L. Gea, P. Marrero, and D. P. Norton, Mat. Res. Soc. Symp. Proc. 401, 203 (1996).

[20] P. E. Blöchl, Phys. Rev. B 50, 17953 (1994).

[21] G. Kresse and J. Furtmuller, Phys. Rev. B 54, 11169 (1996).

[22] G. Kresse and D. Joubert, Phys. Rev. B 59, 1758 (1999).

[23] W. Kohn and L. J. Sham, Phys. Rev. 140, A1133 (1965).

[24] V. I. Anisimov, F. Aryasetiawan, and A. I. Liechtenstein, J. Phys. Condens. Matter 9, 767 (1997).

[25] S. L. Dudarev, G. A. Botton, S. Savrasov, C. J. Humphreys, and A. P. Sutton, Phys. Rev. B 57, 1505 (1998).

[26] H. J. Monkhorst and J. D. Pack, Phys. Rev 13, 5188 (1967).

[27] P. E. Blöchl, O. Jepsen, and O. K. Andersen, Phys. Rev. B 49, 16223 (1994).

[28] I. I. Mazin and D. J. Singh, Phys. Rev. B 56, 2556 (1997).

[29] A. T. Zayak, X. Huang, J. B. Neaton, and Karin M. Rabe, Phys. Rev. B 74, 094104 (2006).

[30] A. T. Zayak, X. Huang, J. B. Neaton, and Karin M Rabe, Phys. Rev. B 77, 214410 (2008).

[31] E. Moreira, J.M. Henriques, D.L. Azevedo, E.W.S. Caetano, V.N. Freire, E.L. Albuquerque, JSSC 184. 921 (2011).

[32] G. Santi and T. Jarlborg, J. Phys. Condens. Matter 9, 9563 (1997).

[33] J. Okamoto, T. Mizokawa, A. Fujimori, I. Hase, M. Nohara, H. Takagi, Y. Takeda, and M. Takano, Phys. Rev. B 60, 2281 (1999).

[34] D. Toyota, Appl. Phys. Lett. 87, 162508 (2005).

국문 초록

이 논문에서, 우리는 강자성 반쪽금속의 후보 물질인 $SrRuO_3$의 전자구조와 물성에 대해서 연구하였다. 우리는 $SrRuO_3$의 띠 구조를 조절해서 강자성 반쪽금속의 바닥상태로 만드는 두 가지 방법을 제시하고자 한다.

첫 번째 방법은 주석 원자를 루테늄 원자의 자리로 도핑을 하는 것이다. 루테늄의 $4d$-궤도전자의 띠와 주석의 $5s$-궤도전자의 띠가 서로 절묘하게 자리잡고 있어서 약간의 루테늄 $4d$-궤도전자의 띠 폭 감소만으로 $SrRuO_3$ 의 반쪽금속 밴드구조를 얻을 수 있다. $Sr(Ru_{1-x}Sn_x)O_3$ 의 합금구조에 대해서 제일원리 전자구조 계산을 수행하였고 LSDA+U 방법론을 적용하였으며 루테늄의 $4d$-궤도전자에 대한 U_{eff} 값으로 1.0 eV 를 사용하였다. $Sr(Ru_{1-x}Sn_x)O_3$ 의 합금구조의 전자구조와 전자의 에너지 밀도 분포를 x = 1/8, 1/4, 1/2, 5/8, 3/4, 7/8 에 대해서 보였다. 그 결과로부터 루테늄의 t_{2g} majority 띠 폭이 주석의 도핑에 따라 감소하는 것을 관찰할 수 있었다. 주석의 $5s$-궤도전자의 띠는 루테늄의 $4d$-궤도전자와 겹치지 않기 때문에 이웃한 원자로 루테늄의 전자의 뜀이 줄어들게 되어서 띠 폭이 줄어든 것이다. 또한 우리는 고정된 주석 도핑비율에 대해서 생길 수 있는 B-자리의 무질서도에 대해서도 분석을 하였다. 정육면제 perovskite 구조의 2×2×2 배에 해당되는 초격자를 구성하고 고정된 주석 도핑비율에서

가능한 모든 B-자리 무질서도의 조합을 계산하였다. 주석이 서로 뭉쳐진 형태의 구조에서는 균일하게 분포한 형태의 구조보다 띠 폭의 분산도가 더 크게 나타났다. 각각의 주석 도핑된 비율에 대해서 모든 가능한 조합의 무질서한 구조의 전자의 에너지 밀도 분포를 더해서 보면 반쪽금속으로의 상태변화를 더 정확히 관찰할 수 있다. 계산된 결과에서 주석 도핑이 $0.6 < x < 0.75$ 의 범위일 때 강자성 반쪽금속의 바닥상태를 보여주었고 0.75 의 주석 도핑에서 금속 절연체 전이가 일어났다. 스핀-궤도 결합을 포함한 계산을 수행하였을 때 체스판 구조의 B-자리 무질서 형태에서 스핀의 방향이 동일선상이 아닌 결과가 나왔지만 그 형태의 총 에너지의 크기가 평면구조의 무질서 형태에 비해서 0.6 eV 만큼 크게 나타났다.

두번째 방법은 적층 방향으로 변형을 가하는 것이다. 격자 크기를 변화시키면 그 물질의 에너지 띠 폭을 조절할 수 있는데, SrRuO3의 경우에 9%의 균일한 부피팽창이 반쪽금속의 바닥상태를 가져오는 것을 발견하였다. 실험에서 서로 다른 격자크기를 자기는 기판물질의 선택을 통해 적층 방향의 변형을 다양한 범위에서 가할 수 있다. 더 정확한 격자상수의 값을 얻기 위해 고체의 물성을 더 정확히 기술하기 위해 개량된 PBEsol 범함수를 사용하여 계산을 하였다. 적층 방향으로 2.5%씩 늘어나는 변형을 가했을 때 루테늄의 t_{2g} 띠 폭이 가장 많이 줄어들었고 LSDA+U 방법과 PBEsol+U 에서 모두 일치하는 결과를 얻었다. 우연하게도 적층 방향으로 2.5%씩 늘어난 $SrRuO_3$의 격자크기는 이전에 연구에서 도핑물질로 사용된 $SrSnO_3$의 격자크기와 가장 비슷하였다.

이 연구는 페로브스카이트 물질에서 반쪽금속을 찾는 데 있어 새로운

가능성을 제시한다. 스핀트로닉스 기술에서 반쪽금속이 가지는 잠재력이 매우 크기 때문에, 주석이 도핑된 SrRuO3 반쪽금속이 실험적으로 구현된다면 스핀트로닉스 소자와 기술의 발전에 이바지 할 수 있을 것이라 생각된다.

주요어: 강자성 반쪽금속, 페로브스카이트 산화물, 범밀도함수론 계산, 온사이트 쿨롱 상호작용, $SrRuO_3$

학번: 2004-30166